AD

USAAVLABS TECHNICAL REPORT 65-69

A THEORY FOR VTOL PROPELLER OPERATION IN A STATIC CONDITION

By

J. C. Erickson, Jr.
R. M. Ladden
H. V. Borst
D. E. Ordway

October 1965

U. S. ARMY AVIATION MATERIEL LABORATORIES
FORT EUSTIS, VIRGINIA
CONTRACT DA 44-177-AMC-165(T)
CURTISS-WRIGHT CORPORATION, VTOL SYSTEMS DIVISION
AND
THERM ADVANCED RESEARCH, INC.

DDC Availability Notices

Qualified requesters may obtain copies of this report from DDC.

This report has been furnished to the Department of Commerce for sale to the public.

Disclaimers

The findings in this report are not to be construed as an official Department of the Army position, unless so designated by other authorized documents.

When Government drawings, specifications or other data are used for any purpose other than in connection with a definitely related Government procurement operation, the United States Government thereby incurs no responsibility nor any obligation whatsoever; and the fact that the Government may have formulated, furnished, or in any way supplied the said drawings, specifications, or other data is not to be regarded by implication or otherwise as in any manner licensing the holder or any other person or corporation, or conveying any rights or permission, to manufacture, use, or sell any patented invention that may in any way be related thereto.

Trade names cited in this report do not constitute an official indorsement or approval of the use of such commercial hardware or software.

Disposition Instructions

Destroy this report when it is no longer needed. Do not return it to the originator.

DEPARTMENT OF THE ARMY
U. S. ARMY AVIATION MATERIEL LABORATORIES
FORT EUSTIS, VIRGINIA 23604

This report has been reviewed by the U. S. Army Aviation Materiel Laboratories for its content. The report is published for the exchange of information and the stimulation of ideas.

1M1.21401D14415
Contract DA44-177-AMC-165(T)
USAAVLABS Technical Report 65-69
October 1965

A THEORY FOR VTOL PROPELLER OPERATION IN A STATIC CONDITION

by

J. C. Erickson, Jr., R. M. Ladden, H. V. Borst & D. E. Ordway

Prepared by

Curtiss-Wright Corporation, VTOL Systems Division
Caldwell, New Jersey

and

Therm Advanced Research, Inc.
Ithaca, New York

for

U. S. ARMY AVIATION MATERIEL LABORATORIES
FORT EUSTIS, VIRGINIA

SUMMARY

The successful design of a propeller-type V/STOL aircraft requires the precise calculation and associated optimization of the propeller performance at the static condition. A general theory for performance calculations has been formulated based on a continuous vortex representation along the lines of the classical lifting-line model.

As opposed to forward flight, the deformation of the wake is appreciable just behind the propeller, and its determination constitutes the heart of the static problem.

A computer program has been developed to calculate both the inflow at the propeller and the induced velocity at any field point for an arbitrary description of the trailing vortex sheets. To approximate the force-free condition imposed on the wake, an initial wake hypothesis derived from the theory of the Generalized Actuator Disk was first used. The resulting comparisons with both detailed and gross measurements were unsatisfactory and a refined hypothesis was derived.

The refined wake hypothesis provides a more reasonable representation of the "pitch" of the elements of the deformed trailing vortex sheets as well as the envelope of their trajectories. Using this hypothesis, comparisons at one power coefficient show excellent agreement with test data, the discrepancy in thrust and pitch setting being about 1% and 2% respectively, and the discrepancy in the figure of merit being about 1% .

PREFACE

The study presented in this report was undertaken by Curtiss-Wright Corp. (C-W), VTOL Systems Division, Caldwell, N. J., as the prime contractor and by Therm Advanced Research, Inc. (TAR), Ithaca, N. Y., as the subcontractor. The study was sponsored by the U. S. Army Aviation Materiel Laboratories (USAAVLABS), Fort Eustis, Va. The authorized representative of the contracting officer was J. E. Yeates.

This is the final report prepared under the contract. The program was carried out under the supervision of H. V. Borst of C-W and D. B. Ordway of TAR. The principal investigators were R. M. Ladden of C-W and J. C. Erickson, Jr. of TAR. These four people are coauthors of this final report. A. L. Kaskel of TAR also participated extensively in this study. Work began in June 1964 and was completed in May 1965.

BLANK PAGE

CONTENTS

ILLUSTRATIONS

SYMBOLS

AF	activity factor of propeller blade, Eq. (27)
b	local propeller blade chord, feet
C_L	blade sectional lift coefficient, Eq. (12)
C_{L_i}	blade sectional design lift coefficient
C_P	power coefficient of propeller, Eq. (17)
C_T	thrust coefficient of propeller, Eq. (16)
D_B	distance from bound vortex element $(0,r_p,\theta_p)$ to field point (x,r,θ), Table 1
D_T	distance from trailing vortex element (x_v,r_v,θ_v) to field point (x,r,θ), Table 1
dD	elemental profile drag on blade section, Fig. 2
dL	elemental lift on blade section, Fig. 2
$-d\Gamma$	strength of vortex sheet element trailing from $(0,r_p,\theta_p)$, Fig. 1
F/M	figure of merit, Eq. (18), percent
G_ℓ	ℓ^{th} nondimensional Glauert coefficient in representation of Γ, Eq. (22)
h/b	local propeller blade thickness-to-chord ratio
IC_{L_i}	integrated design lift coefficient of propeller blade, Eq. (28)
K_u	iteration factor chosen to achieve convergence of axial component of induced velocity field, Eq. (19)
K_v	corresponding factor for radial component, Eq. (20)
K_w	corresponding factor for tangential component, Eq. (21)
$\mathscr{L}$	number of Glauert coefficients used in representation of Γ, Eq. (22)

N	number of propeller blades
$\mathcal{O}_u$	Biot-Savart operator for axial induced velocity component, Eq. (9)
$\mathcal{O}_v$	corresponding operator for radial component, Eq. (10)
$\mathcal{O}_w$	corresponding operator for tangential component, Eq. (11)
P	total power absorbed by propeller, horsepower
R_h	propeller hub radius, feet
R_p	propeller tip radius, $D_p/2$, feet
r	radial coordinate, Fig. 1
r_p	radial coordinate along p^{th} propeller blade, Fig. 1
r_v	radial coordinate along trajectory of vortex sheet element trailing from $(0,r_p,\theta_p)$, Fig. 1 and Eq. (7)
$\mathcal{S}_u$	singular part of $\mathcal{U}_T$, Eq. (24)
$\mathcal{S}_v$	singular part of $\mathcal{V}_T$, Eq. (25)
$\mathcal{S}_w$	singular part of $\mathcal{W}_T$, Eq. (26)
T	total propeller thrust, pounds
t	parametric time for a fluid particle to move along a trailing vortex trajectory
$\mathcal{U}_B$	influence function for the axial component of velocity induced at (x,r,θ) by a bound radial vortex element of unit strength and unit length at $(0,r_p,\theta_p)$, Table 1
$\mathcal{U}_T$	influence function for axial component of velocity induced at (x,r,θ) by an arbitrarily deformed vortex sheet element of unit strength and semi-infinite length trailing from $(0,r_p,\theta_p)$, Table 1
u	axial component of velocity induced at (x,r,θ), taken positive in the positive x-direction, Eq. (2)
u_p	axial inflow component at $(0,r_p,\theta_p)$, Fig. 2

u_v	axial velocity component at (x_v, r_v, θ_v)
$\mathcal{V}_B$	radial counterpart of $\mathcal{U}_B$, Table 1
$\mathcal{V}_T$	radial counterpart of $\mathcal{U}_T$, Table 1
v	radial component of velocity induced at (x,r,θ) taken positive in positive r-direction, Eq. (3)
v_p	radial inflow component at $(0, r_p, \theta_p)$
v_v	radial velocity component at (x_v, r_v, θ_v)
$\mathcal{W}_B$	tangential counterpart of $\mathcal{U}_B$, Table 1
$\mathcal{W}_T$	tangential counterpart of $\mathcal{U}_T$, Table 1
W_p	total velocity seen by blade section, Fig. 2
w	tangential component of velocity induced at (x,r,θ), taken positive in positive θ-direction, Eq. (4)
w_p	tangential inflow component at $(0, r_p, \theta_p)$, Fig. 2
w_v	tangential velocity component at (x_v, r_v, θ_v)
x	axial coordinate, Fig. 1
x_v	radial coordinate along trajectory of vortex sheet element trailing from $(0, r_p, \theta_p)$, Fig. 1 and Eq. (6)
α	local blade angle of attack, Fig. 2, degrees
β	local blade pitch setting, Fig. 2, degrees
Γ	local bound blade circulation strength
γ	tangent angle of sectional lift-drag polar, Fig. 2
Δt	time increment in marching scheme for trajectory determination
θ	azimuthal coordinate, Fig. 1
θ_p	azimuthal coordinate of p^{th} propeller blade, Eq. (1)
θ_v	azimuthal coordinate along trajectory of vortex sheet element trailing from $(0, r_p, \theta_p)$, Fig. 1 and Eq. (8)

ϑ_p Glauert variable running from 0 to π with center midway between propeller hub and tip, Eq. (23)

ρ fluid density

ϕ_p angle between r_p and W_p, Fig. 2

Ω angular speed of propeller, Fig. 1, $2\pi n$, radians per second

INTRODUCTION

The design of high-performance propellers for V/STOL aircraft has been hindered by the lack of a suitable theory for the determination of performance at the hover operating condition. This theory is needed for calculating the inflow velocity at each blade station so that two-dimensional airfoil data can be applied to find the overall thrust and obtain the design characteristics of the blade for peak overall airplane performance. The static performance of conventional propellers has not been a critical design condition.

The static thrust generated by conventional propellers has been calculated using single point methods based on full-scale propeller test data. These procedures do not show how detailed blade geometry changes affect the overall performance and, therefore, are not suitable for blade design studies. To overcome this difficulty, attempts were made to extrapolate the theory for the forward flight condition to the zero speed case and then calculate the inflow velocity. This procedure appeared to be suitable for conventional propeller design purposes, but it did not have the necessary accuracy for use in designing propellers for V/STOL aircraft.

The need for peak propeller performance with V/STOL aircraft is greater than with conventional aircraft as the propellers must generate a total lift equal to the gross weight of the aircraft. Since the payload of these vehicles is 20% to 30% of the gross weight, a small improvement in the lift or hover performance of the propellers results in a large improvement in payload capacity. High levels of cruise efficiency must also be obtained to keep the fuel weight requirements to a minimum.

The principal difficulty in computing the inflow velocity in the static case is locating the trailing vortex elements. The position of the elements in the wake is determined by the propeller rotation and the velocities generated by the blades; i.e., these elements must deform such that they are force free. At the forward flight condition, however, the wake position is determined mainly by the propeller rotation and the axial free stream velocity. Thus, in forward flight the position of the wake is known based on the operating condition, whereas in the static case the position of the wake is unknown. Since the inflow is extremely sensitive to the wake position, the deformation of the trailing vortex elements must be found precisely for the elements near the blade station at which the

inflow is being evaluated. This is especially important for the outboard stations, where small changes have the most significant effect on the performance.

The complicated interaction between the wake and the inflow as described makes it necessary to use the process of iteration to solve the problem. Thus for an assumed load distribution and wake deformation, the inflow is calculated and so from two-dimensional airfoil data a new load distribution is obtained. With the new load distribution, a new wake deformation is computed and the process repeated until reasonable convergence is realized.

Since the propeller and the turbine engine are an effective lightweight system for providing both hover lift and propulsion at cruise for V/STOL aircraft, the ability to design the optimum configuration is of considerable importance. To fill the existing void, a theoretical program was undertaken so that the necessary data could be calculated for use in the design of propellers. Effort was made to apply all available test data as a guide for the analysis as well as a check on the results. The experience gained from the development and use of the forward flight theory was employed to keep the program practical and useful.

CHAPTER 1

THEORETICAL FORMULATION

Basic Equations

We consider a propeller rotating at a constant angular speed Ω in a uniform, inviscid fluid which has a density ρ and is at rest at infinity. The blade thickness-to-chord and chord-to-radius ratios are assumed to be sufficiently small that the classical lifting-line formulation is a reasonable approximation. We can then represent the propeller blades by radial bound vortex lines accompanied by a force-free system of trailing vortex sheets.

A propeller-fixed cylindrical coordinate system (x,r,θ) is chosen with the axis of rotation as the x-axis, see Fig. 1 . The N blades are located in the plane $x = 0$ and arranged symmetrically such that

$$\theta_p = 2\pi(p-1)/N \qquad p = 1, 2, \ldots, N \tag{1}$$

i.e., the $p = 1$ blade coincides with $\theta = 0$.

The induced velocity anywhere in the propeller field is determined by integration of the Biot-Savart law over all the vortex elements comprising the system in terms of their strength, orientation and distance to the field point of interest, and may be expressed in the form

$$u = \sum_{p=1}^{N} \int_{R_h}^{R_p} \left[\Gamma(r_p)\, \mathscr{U}_B - \frac{d\Gamma(r_p)}{dr_p}\, \mathscr{U}_T \right] dr_p \tag{2}$$

$$v = \sum_{p=1}^{N} \int_{R_h}^{R_p} \left[\Gamma(r_p)\, \mathscr{V}_B - \frac{d\Gamma(r_p)}{dr_p}\, \mathscr{V}_T \right] dr_p \tag{3}$$

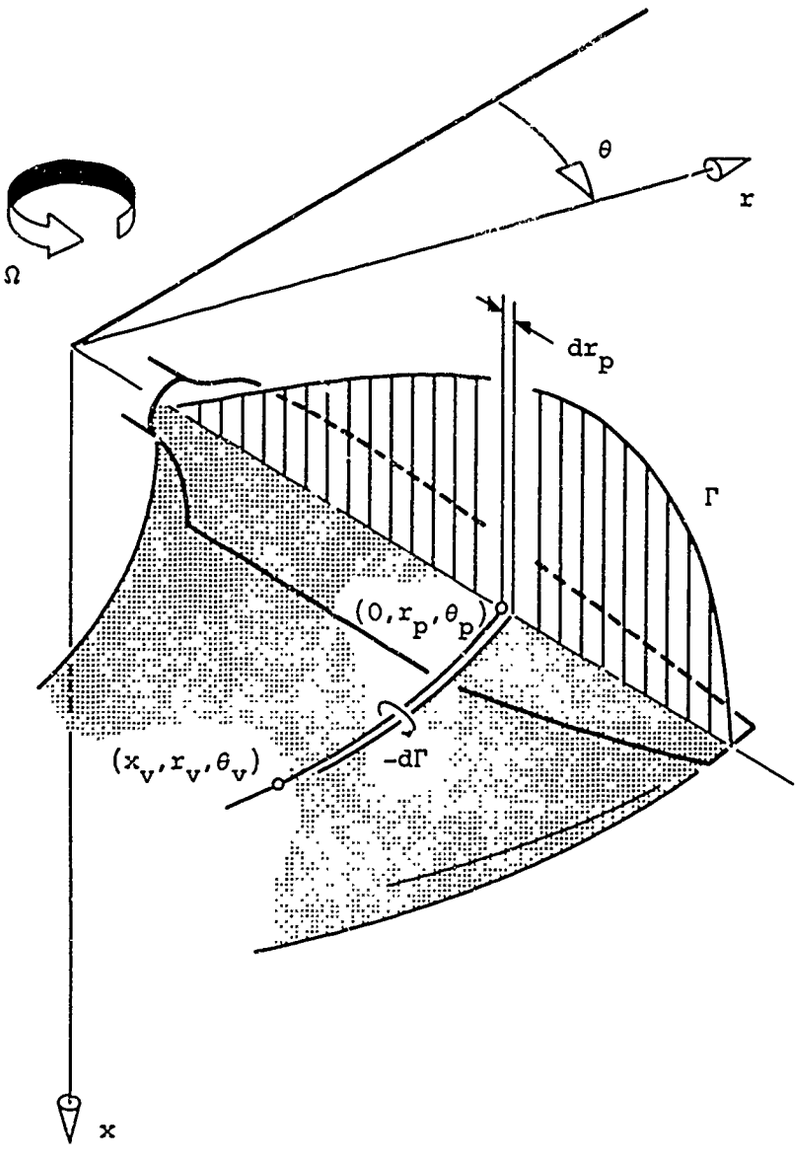

Figure 1. Propeller Coordinates and Vortex Representation.

$$w = \sum_{p=1}^{N} \int_{R_h}^{R_p} \left[\Gamma(r_p)\, \mathscr{W}_B - \frac{d\Gamma(r_p)}{dr_p}\, \mathscr{W}_T \right] dr_p \qquad (4)$$

where

u is the axial component of the velocity induced at a field point (x,r,θ) and taken positive in the positive x-direction,

v is the corresponding radial component, positive in the positive r-direction, and

w is the corresponding tangential component, positive in the positive θ-direction;

R_h is the radius of the propeller hub;

R_p is the radius of the propeller tip;

Γ is the bound blade circulation strength at $(0,r_p,\theta_p)$;

$-d\Gamma$ is the strength of the vortex sheet element trailing from $(0,r_p,\theta_p)$;

r_p is the radial variable of integration along the p^{th} propeller blade;

$\mathscr{U}_B$ is the influence function for the axial component of the velocity induced at (x,r,θ) by a bound radial vortex element of unit strength and unit length at $(0,r_p,\theta_p)$,

$\mathscr{V}_B$ is the corresponding function for the radial component, and

$\mathscr{W}_B$ is the corresponding function for the tangential component; and

$\mathscr{U}_T$ is the influence function for the axial component of the velocity induced at (x,r,θ) by an arbitrarily deformed vortex sheet element of unit strength and semi-infinite length trailing from $(0,r_p,\theta_p)$,

$\mathscr{V}_T$ is the corresponding function for the radial component, and

$\mathcal{W}_T$ is the corresponding function for the tangential component.

The influence functions can be derived from first principles (Ref. 24, pp. 1.10 to 1.12, for example) or obtained from previous results (Ref. 20, pp. 13 to 16). They are summarized in Table 1 where

x_v is the axial coordinate of any point on the trajectory of the vortex sheet element trailing from $(0, r_p, \theta_p)$,

r_v is the corresponding radial coordinate, and

θ_v is the corresponding angular coordinate;

u_v is the value of u at (x_v, r_v, θ_v) ,

v_v is the corresponding value of v , and

w_v is the corresponding value of w ; and

t is a time parameter to be defined.

When a point on a blade is chosen as a field point, the contribution from the bound vortex for this blade is irrelevant and so discarded, as in wing theory (Ref. 13, pp. 131 to 133).

The contribution from the bound vortices to the induced velocity is simple to calculate. The contribution to the induced velocity from the elements of the trailing vortex sheets, on the other hand, is very complicated. Not only do the influence functions require an integration over the length of the element, but what is even worse, the location or "trajectory" of the element is not fixed. Rather, these elements must drift force free by aligning themselves with the streamlines of the flow, which in differential form (Ref. 24, pp. 1.1 to 1.2, for example) are

$$\frac{dx}{u} = \frac{dr}{v} = \frac{d\theta}{\Omega+(w/r)} \tag{5}$$

These equations can be integrated in terms of the parametric time t that it takes a fluid particle to move along this trajectory, giving

TABLE 1

SUMMARY OF INFLUENCE FUNCTIONS

$$\mathscr{U}_B = - r \sin(\theta_p-\theta)/4\pi D_B^3$$

$$\mathscr{V}_B = x \sin(\theta_p-\theta)/4\pi D_B^3$$

$$\mathscr{W}_B = - x \cos(\theta_p-\theta)/4\pi D_B^3$$

$$D_B \equiv [r_p^2 + r^2 - 2r_p r \cos(\theta_p-\theta) + x^2]^{\frac{1}{2}}$$

$$D_T \equiv [r_v^2 + r^2 - 2r_v r \cos(\theta_v-\theta) + (x_v-x)^2]^{\frac{1}{2}}$$

$$\mathscr{U}_T = \int_0^\infty \frac{- v_v r \sin(\theta_v-\theta) + (\Omega r_v+w_v)[r_v-r\cos(\theta_v-\theta)]}{4\pi D_T^3}\, dt$$

$$\mathscr{V}_T = \int_0^\infty \frac{u_v r_v \sin(\theta_v-\theta) - v_v(x_v-x)\sin(\theta_v-\theta) - (\Omega r_v+w_v)(x_v-x)\cos(\theta_v-\theta)}{4\pi D_T^3}\, dt$$

$$\mathscr{W}_T = \int_0^\infty \frac{- u_v[r_v\cos(\theta_v-\theta) - r] + v_v(x_v-x)\cos(\theta_v-\theta) - (\Omega r_v+w_v)(x_v-x)\sin(\theta_v-\theta)}{4\pi D_T^3}\, dt$$

$$x_v = \int_0^t u_v \, d\tau \tag{6}$$

$$r_v = r_p + \int_0^t v_v \, d\tau \tag{7}$$

$$\theta_v = \theta_p + \Omega t + \int_0^t (w_v/r_v) \, d\tau \tag{8}$$

The integrands in Eqs. (6) to (8) are functions of the coordinates along the trajectory and the coordinates themselves are functions of t .

For convenience, we now introduce a set of operators such that Eqs. (2) to (4) become simply

$$u = \mathcal{O}_u(\Gamma, -d\Gamma/dr;\ u,v,w) \tag{9}$$

$$v = \mathcal{O}_v(\Gamma, -d\Gamma/dr;\ u,v,w) \tag{10}$$

$$w = \mathcal{O}_w(\Gamma, -d\Gamma/dr;\ u,v,w) \tag{11}$$

where

- $\mathcal{O}_u$ is the Biot-Savart operator for the axial induced velocity component,
- $\mathcal{O}_v$ is the corresponding operator for the radial component, and
- $\mathcal{O}_w$ is the corresponding operator for the tangential component.

Note carefully that the operators operate on the bound and

trailing vortex strengths with the velocity field itself as a parameter. These equations constitute a set of simultaneous, nonlinear, singular integral equations over the domain of the blades and the trailing vortex sheets. This set is complete if Γ is specified.

If Γ is not specified, another equation is required to relate the circulation strength and velocity field through the propeller geometry. Consider the force and velocity diagram for a typical section of the blade at the radial station $(0,r_p,\theta_p)$, see Fig. 2 , where

W_p is the total local velocity seen by the blade section;

u_p is the local axial inflow, i.e. the axial component of the induced velocity at $(0,r_p,\theta_p)$,

v_p is the corresponding radial inflow (not shown, but perpendicular to the plane of the section), and

w_p is the corresponding tangential inflow;

α is the local blade angle of attack;

β is the local blade pitch setting;

ϕ_p is the angle between Ωr_p and W_p ;

γ is the tangent angle of the sectional lift-drag polar;

dD is the elemental profile drag on the blade section; and

dL is the elemental lift on the blade section.

From the definition of the sectional lift coefficient in terms of the local blade chord b ,

$$C_L \equiv 2(dL/dr_p)/\rho W_p^2 \, b \qquad (12)$$

the Kutta-Joukowski formula (Ref. 24, pp. 5.21 to 5.22, for example) can be written as

$$\Gamma = b \, W_p \, C_L/2 \qquad (13)$$

$$W_p \equiv [u_p^2 + (\Omega r_p + w_p)^2]^{\frac{1}{2}}$$

$$\alpha \equiv \beta - \phi_p$$

$$\phi_p \equiv \tan^{-1}[u_p/(\Omega r_p + w_p)]$$

$$\gamma \equiv \tan^{-1}(dD/dL)$$

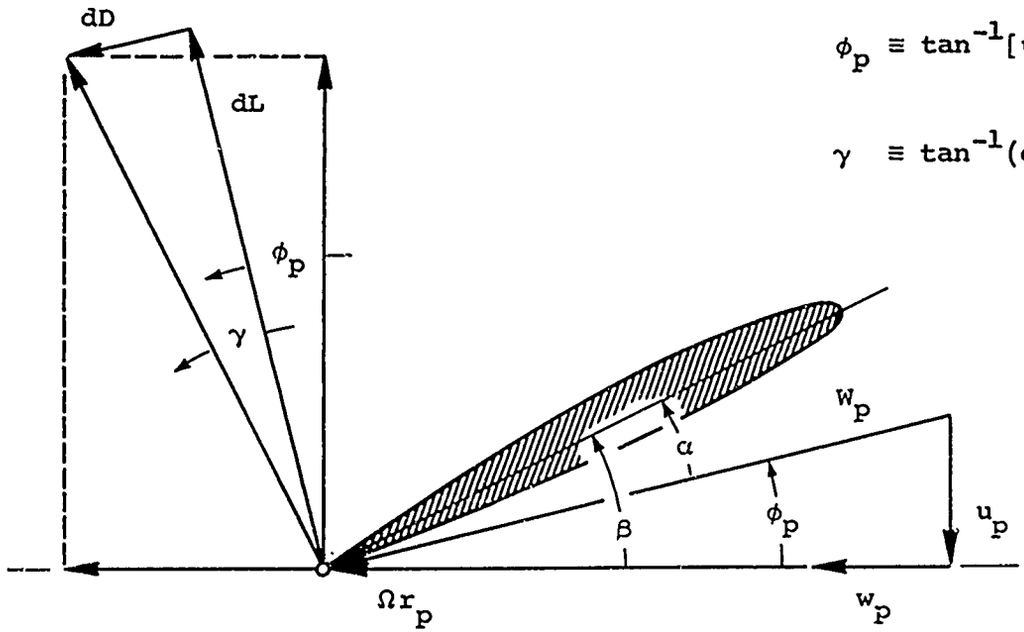

Figure 2. Velocity and Force Diagram at Typical Section.

where the lift coefficient is assumed known (Ref. 7) as a function of α for a given section at approximately the local Mach and Reynolds numbers. This is the equation needed in conjunction with Eqs. (9) to (11) to complete the set when the propeller geometry is specified.

In either case, the circulation or the propeller geometry specified, the prediction of the overall performance can be computed once the inflow has been calculated. In particular, if we resolve the resultant of dL and dD as indicated by the dotted lines in Fig. 2 and integrate along the blade for the N blades, the total thrust T and power P in non-dimensional form are

$$C_T = \frac{\pi^2 N}{8} \int_{R_h/R_p}^{1} C_L \frac{\cos(\phi_p+\gamma)}{\cos\gamma} \left(\frac{W_p}{\Omega R_p}\right)^2 \frac{b}{R_p} d\left(\frac{r_p}{R_p}\right) \tag{14}$$

$$C_P = \frac{\pi^3 N}{8} \int_{R_h/R_p}^{1} C_L \frac{\sin(\phi_p+\gamma)}{\cos\gamma} \left(\frac{W_p}{\Omega R_p}\right)^2 \frac{b}{R_p} \frac{r_p}{R_p} d\left(\frac{r_p}{R_p}\right) \tag{15}$$

where the thrust and power coefficients of the propeller are defined by

$$C_T \equiv \pi^2 T/4\rho\Omega^2 R_p^4 = T/\rho n^2 D_p^4 \tag{16}$$

$$C_P \equiv \pi^3 P/4\rho\Omega^3 R_p^5 = P/\rho n^3 D_p^5 \tag{17}$$

respectively, with $\Omega = 2\pi n$ and $R_p = D_p/2$.

From the thrust and power coefficients we can calculate the figure of merit F/M (Ref. 19, pp. 353 to 355), given in percent, by

$$F/M \equiv 100\sqrt{2C_T^3/\pi C_P^2} = 79.8\ C_T^{3/2}/C_P \tag{18}$$

To conclude this section, it is of interest to discuss the nondimensionalization of the basic equations of the static thrust problem. As we have implied by the form of Eqs. (16) and (17), the characteristic time is $1/\Omega$ and the characteristic length is R_p. If the equations are nondimensionalized with respect to these quantities, complete similarity exists with the exception of the sectional lift and drag data which in general must include the effects of Mach number and Reynolds number, as noted earlier.

Outline of Solution

The set of equations described above cannot be solved analytically, so approximate numerical techniques must be employed. Iteration is perhaps the most straightforward approach and the one which we have chosen.

First we rewrite Eqs. (9) to (11) in a different, but equivalent, form, namely

$$u = u - K_u[u - \mathcal{O}_u(\Gamma, \ \ldots \ )] \tag{19}$$

$$v = v - K_v[v - \mathcal{O}_v(\Gamma, \ \ldots \ )] \tag{20}$$

$$w = w - K_w[w - \mathcal{O}_w(\Gamma, \ \ldots \ )] \tag{21}$$

where

K_u is a factor chosen as necessary to achieve convergence of the axial component of the induced velocity field,

K_v is the corresponding factor for the radial component and

K_w is the corresponding factor for the tangential component.

These iteration factors may be constant or may depend on any of the variables of the problem.

With the propeller geometry specified, iteration begins by finding a zeroth, or initial, approximation to the inflow and so the blade circulation through Eq. (13), the Kutta-Joukowski formula. The first approximation to the inflow follows by operating with the Biot-Savart operator on the zeroth approximation to the blade circulation and some guess at the induced velocity field in the propeller wake. These results, along with the iteration factors and the zeroth approximations to the inflow and the wake velocity field, are then substituted into the right-hand sides of Eqs. (19) to (21) to give the first approximations to the inflow and the wake velocity field, respectively. The iteration continues by operating as before on the first approximation to determine a second, and so forth. Once convergence within a prescribed accuracy is reached, the propeller performance can be calculated.

For the case with the blade circulation specified, on the other hand, iteration would proceed similarly except that the circulation would not change at each step. Upon convergence, the blades could be designed consistent with the Kutta-Joukowski formula and the performance calculated.

The iteration approach necessitates, at each step of the iteration, calculation of the induced velocity field at a sufficient number of points to define accurately the local streamlines in the propeller wake. Unfortunately, the number of calculations required for adequate representation of the complete distributed vortex sheets is very large. As a result, we looked for some way which would reduce the number of calculations but still satisfy the force-free condition of the wake, at least in an approximate sense.

The question of convergence and the proper choice of the iteration factors in Eqs. (19) to (21) present a major difficulty. Standard methods to guarantee convergence (Ref. 27, for example) are not feasible for calculations of this scope. We will elaborate more on convergence later.

Pitchfork Model

When our original investigation was undertaken in October 1962, little experimental information was available on the detailed nature of the propeller wake deformation, other than a few smoke pictures. Consequently, we turned to intuitive considerations for a plausible wake behavior. Based upon

order-of-magnitude studies using results from finite wing theory, we hypothesized that roll up of the trailing vortex sheet from each blade into a pair of concentrated vortices was the predominant feature of the wake and formulated our so-called "Pitchfork Model" (Ref. 22). This model treated roll up in a simple fashion by assuming that the trailing vortex sheet from each blade was completely undeformed axially and radially until the inboard and outboard roll-up points were reached, whereupon the respective portions of the sheet were assumed to contract discontinuously, i.e. to roll up instantaneously, to a pair of concentrated vortices.

The Biot-Savart operator appropriate to this model was programmed in steps for numerical computation on the CDC 1604 digital computer at the Cornell University Computing Center (Refs. 22 and 8). First approximations in the iteration were calculated at three pitch settings of the 3(10188A2P2) propeller (Refs. 9 and 10). At one of these settings a parametric study of the effects of roll-up point variation on the first approximation was made (Ref. 9) and a second approximation was calculated for the most promising of these (Ref. 10). The results indicated that the Pitchfork Model was indeed a step towards an improved theory, and gave good qualitative indications of the effect of overall contraction.

However, quantitative predictions were impaired greatly by the failure to represent the initial axial and radial deformation of the distributed trailing vortex sheets, especially near the tip. We thus concluded that continuous deformation of the vortex sheets was necessary in an adequate model of the vortex wake. No conclusion about the importance of roll up could be drawn at that time, although the lack of fundamental knowledge of the basic nature of roll up in the propeller case was clear as well as the need for more detailed experimental investigations to improve the wake model.

Continuous Deformation Model

When the present theoretical investigation was initiated, we reviewed extensively previous theories for propellers in forward flight with the specific aim of gaining a better understanding of the overall nature of the trailing vortex sheet deformation (Ref. 6, pp. 218 to 222; Ref. 18; Ref. 26, pp. 77 to 87; Refs. 28 and 14). In general, the sheets stretch axially, together with a radial contraction and a tangential distortion. The edges of the sheets are also locally unstable and tend to roll up as for a finite wing.

While these deformations are not of primary significance for the practical determination of aircraft propeller performance in forward flight (Ref. 3), they are the heart of the static problem. Without a free stream, not only do the deformations occur much closer to the propeller and so exert more influence, but they are also much larger. In fact, the axial elongation which is only a perturbation of the basic helical sheets in forward flight is now the total variation itself.

Simultaneously, we turned to the new experimental knowledge of the wake that was available in the summer of 1964. We had taken photographs of the condensation paths of the tip vorticity. Also, Canadair, Ltd. had made new smoke visualization studies.

Based upon these results and the above discussions, we decided to concentrate upon the continuous axial stretching and radial deformation of the trailing vortex sheets, or in other words, a "Continuous Deformation Model". At the same time, we concluded that it was important to provide for incorporation of the effect of roll up, if necessary, at a later date.

Inasmuch as the associated development of a satisfactory approximation to the force-free condition of the wake continued throughout the investigation, we will defer the details until the calculations for the specific propellers are described.

CHAPTER 2

METHOD OF CALCULATION

Implementation

In order to carry out the iterative solution which we have outlined, a general computer program was developed to evaluate the induced velocity field given by Eqs. (2) to (4). The remaining calculations involved, namely Eq. (13) and Eqs. (19) to (21), are straightforward and were carried out by hand. Once the inflow at the propeller was established, the resulting predictions of the overall performance expressed by Eqs. (14), (15) and (18) were found by means of a modification of the integration method of the existing C-W strip analysis (Ref. 11). This also was carried out by hand.

In this chapter we will describe the computer program, as well as the associated numerical analyses, and indicate its use to date.

Description of Computer Program

The computer program was made as flexible as possible to provide a "working tool" for handling whatever details we might wish to incorporate as the study progressed. It can treat an arbitrary, continuous deformation of the trailing vortex sheets, with or without discontinuous roll up into discrete vortices. If present, roll up can occur either outboard, inboard, or both outboard and inboard. The discrete vortices themselves are assumed to be regular helices. Their geometry is fixed by the local pitch of the element of the trailing vortex sheet adjoining the roll-up point but the location of this point may be varied. Besides these basic options, alternate routes were included in the program to minimize the running time wherever we could.

The program was written in FORTRAN 63 for the CDC 1604 computer. The particular machine that we used is located at the Cornell University Computing Center. To achieve the flexibility desired, most of the principal operations were relegated to subroutines, leaving the logic for the assorted options as the main framework of the program.

After several runs, we saw that it was important to examine the trajectories of the trailing vortex sheet elements for physical reasonableness without running the full program. Therefore a short program was abstracted to compute just the trajectories. It was generally run before each run of the full program.

From the duplicate FORTRAN 63 decks of both programs which have been cut and supplied to USAAVLABS, complete listings can be made.

In the following we will emphasize the option for continuous deformation without roll up, since this is the one which we used for almost all of our runs. Instructions are provided for the corresponding preparation of input data in Appendix I .

Representation of Circulation Distribution

In general, the blade circulation distribution Γ is tabulated numerically at several radial stations, but for certain of the subsequent integrations we need Γ in analytic form.

A suitable form is a Glauert-type series (Ref. 13, pp. 138 to 139), or

$$\Gamma = \Omega R_p^2 \sum_{\ell=1}^{\mathscr{L}} G_\ell \sin \ell \vartheta_p \tag{22}$$

$$r_p \equiv \tfrac{1}{2}(R_p+R_h) - \tfrac{1}{2}(R_p-R_h) \cos \vartheta_p \tag{23}$$

where

G_ℓ is the ℓ^{th} nondimensional Glauert coefficient; and

ϑ_p is the Glauert variable which runs from 0 to π with its center midway between the hub and tip.

This form possesses a square-root behavior at both the tip and the hub. For the tip this is the proper behavior required for a lifting-line formulation (Ref. 5, pp. 171 to 174, for example). For the hub it is approximately correct when the blade necks down rapidly at the shank as the 3(13168A10P3) propeller does. When the hub is like the root of a wing, on the other hand, the slope of the circulation distribution should be zero from a rigorous viewpoint. This could have been achieved exactly by an additional condition on the determination of the Glauert coefficients, but practically the contribution of the hub to the overall performance is so small that zero slope can be achieved with or without this condition.

There are various ways that the Glauert coefficients can be evaluated. We chose the method of least squares which minimizes the error at the specified data points (Ref. 23, pp. 363 to 370). The program provides for the numerical values of Γ to be given at up to 30 points, with $\mathscr{L}$ as high as 20 . Usually $\mathscr{L} = 15$ was adequate. For a fairly smooth circulation, the worst error at any point was on the order of 1%, and for an irregular shape, about twice as great.

Velocity Induced by Bound Blade Vortices

As is generally known, the contribution of the bound blade vortices to the induced velocity is identically zero at the propeller blades, see Table 1, but is generally nonzero at field points located off the blades. Consequently, the appropriate influence functions are regular throughout the range of interest. This, combined with the algebraic form of these functions and the fixed location of the vortex elements, makes the integration of the first terms of Eqs. (2) to (4) relatively simple.

The integration proceeds as follows. The influence functions are calculated at the radial stations for which the data for the circulation distribution are tabulated. These values are multiplied by the corresponding values of Γ to give a set of values for the integrands. Values of the integrand not contained in this set are found as necessary by 3-point Lagrangian interpolation (Ref. 23, pp. 72 to 73, for example). The integration itself then is carried out over the original radial variable by a generalized Gaussian scheme devised by A. L. Kaskel at TAR, Inc. In this scheme, a 10-point Gaussian quadrature is first applied to the total interval

of integration. The total interval is in turn subdivided into two intervals and the 10-point Gaussian quadrature applied to each of these intervals and the results added to get the answer. Next, the total interval is subdivided into three intervals, and so on. At each step after the second, the answer is compared with the two values which immediately precede it, and the subdivision is continued until these three values are within a desired accuracy.

The accuracy used was $\pm$ 0.00005 of the tip rotational speed. For most of our runs this required 3 to 5 subdivisions of the total interval, or equivalently, the weighting of the integrand at 30 to 50 points.

Velocity Induced by Trailing Vortex Sheets

As pointed out earlier, we must in general calculate the trajectories of the elements of the trailing vortex sheets in order to evaluate the contribution by these sheets to the induced velocity. Physically, most of the wake deformation occurs just downstream of the propeller, say within a distance of a blade radius or so. Integration of Eqs. (6) to (8), therefore, is necessary only in this region. Further downstream the trajectories may be approximated as regular helices with suitable pitch, either distributed or contracted discontinuously into discrete vortices.

To carry out the trajectory integrations, a prescribed velocity field along the trailing vortex sheets, either from a guess or the preceding step of the iteration, has to be stored in the computer as input data. Though the real flow field is not axisymmetric, we can in effect imagine that it is since we only move along a trajectory. In other words, the flow is periodic in θ between the trailing vortex sheets so that u, v and w at any set of values for θ which are $2\pi/N$ apart, at any x and r, are identical. This is illustrated in Fig. 3 for the cross section of the wake of a 3-bladed propeller with the trailing vortex sheets arbitrarily deformed. The actual radial velocity is given by the solid line and the apparent axisymmetric radial counterpart is given by the dotted line.

The stored velocity field is specified at a number of values of x and r and 3-point Lagrangian interpolation, first in r and then in x, carried out for other values in between. For each of 15 radial stations, we took 20 axial stations

between the propeller plane, or slightly upstream when necessary, and some distance downstream.

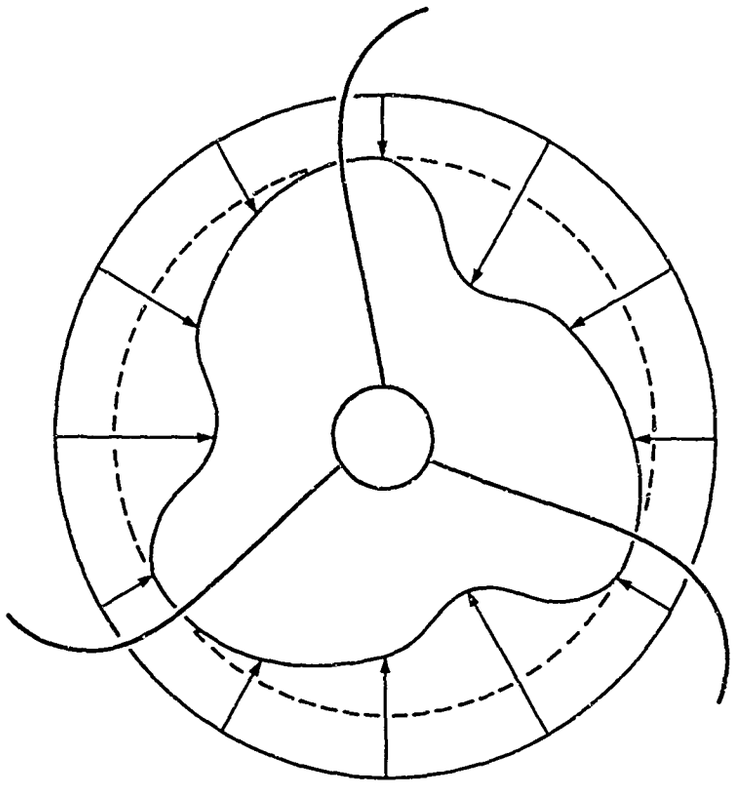

Figure 3. Actual and Axisymmetric Counterpart for Radial Component.

With the velocity field stored, the trajectory can be evaluated in a step-by-step marching scheme using a 2-term constant slope method. The first step off the blade is made by multiplying the inflow components by a small, but arbitrary, time increment Δt to find the new location of the vortex sheet element. The second, and successive, steps are taken by interpolating to determine the velocity at this new location, multiplying it by $2\,\Delta t$ and adding the result to the coordinate of the previous location. With this scheme the error is of the order of the cube of Δt as opposed to

the square of Δt , which an ordinary 2-term Taylor series would afford. The increment Δt is constant as the march proceeds but may be increased to a new value at one point downstream to speed the march.

Simultaneously with this march, it is convenient to perform the integration over t for evaluation of this contribution of the deformed wake to the influence functions, see Table 1 The integrands are calculated at each new location in the march and integrated by Simpson's rule after each two steps. Running totals of the influence functions are carried as the march proceeds.

Assessment of this scheme was made by calculation of an example for which the trajectory was known exactly. Agreement between the exact and approximate trajectories was excellent. In addition, a number of tests on actual trajectories were made with different values of Δt . It was found that the size of Δt was more critical for the integration of the influence functions to a desired accuracy than for the trajectory itself. After evaluation, we chose $\Omega\Delta t = 0.008$ for the initial increment and $\Omega\Delta t = 0.104$ for the second increment. The number of steps at the former was fixed at 58, but the number at the latter is determined by the time taken for the "slowest element" to reach a distance downstream as prescribed by the wake model, see Eq. (6). Usually this was about 100 to 200 steps.

When this prescribed distance is reached, the trajectories become regular helices and Eqs. (6) to (8) could be integrated explicitly because the axial and tangential velocity components in the field are constant and the radial component is zero. This was not done in the present computer program and the contributions of these helical portions to the influence functions were calculated in the same fashion as for the deformed portions.

Since the helical portions extend downstream to infinity, it was necessary to find suitable asymptotic formulas for them. We had concluded from our previous studies that formal asymptotic expansions of the contributions to the influence functions could be made (Ref. 8, p. 17), but an even better choice is the calculation of the θ-average of these contributions (Ref. 8, pp. 18 to 23; Ref. 9, pp. 10, 19 to 20; Ref. 10, p. 21). These contributions to the influence functions can be extracted from the results of the theory of the Generalized Actuator Disk (Ref. 14, pp. 13 to 15). Their calculation involves simply the evaluation of some well-defined

functions, namely the Legendre functions of the second kind and plus and minus one-half order and the Heuman lambda function. We chose to evaluate the Legendre functions by relating them to the complete elliptic integrals of the first and second kinds (Ref. 4, p. 249), which are computed using a rational approximation (Ref. 1, pp. 591 to 592). For the Heuman lambda function we took an exact series expansion (Ref. 4, p. 300) and related it, also, to the complete elliptic integrals of the first and second kind. These integrals are calculated as before. Where applicable, the addition formula for the Heuman lambda function (Ref. 4, p. 36) is employed to speed convergence of the series.

When the calculation of the influence functions is complete, we multiply them by their corresponding trailing vortex strengths and proceed to the integrations of the second terms of Eqs. (2) to (4). Unfortunately, the singularities of the integrand complicate the picture and require special treatment in order to carry out these integrations quickly and accurately.

We first see that the square-root behavior of Eq. (22) makes the strength of the elements of the trailing vortex sheets infinite at the hub and the tip. This is no problem, though, if we carry out the integrations in terms of the Glauert variable instead of the original radial variable, as in finite wing theory. A more serious difficulty is the existence of singularities which arise in the influence functions when the field point coincides with an element of the trailing vortex system. The nature of these singularities can be determined by direct investigation of the equations in Table 1 . In particular, at the lifting line itself the singularities are not integrable for a nonzero value of the radial inflow. This is the same nonintegrable singularity which has arisen in attempts to extend lifting-line theory to swept-back wings (Refs. 12, 25, 17, for example). We handled this difficulty by taking the first two steps in the marching scheme with zero radial velocity and constant axial and tangential velocity, i.e. as regular helical elements, after which the trailing elements deform in the desired fashion. Since Δt is taken so small, this displacement from the lifting line is infinitesimal compared to the blade chord.

As shown elsewhere (Ref. 21, pp. 14 to 16), we are left with two types of singularities, Cauchy and logarithmic. To handle the integration over these singularities, we sum the influence functions over all the blades and break the results into "singular" and "regular" parts. If we define

$$\delta_u \equiv \frac{\Omega r+w}{4\pi[u^2+(\Omega r+w)^2]^{\frac{1}{2}}} \frac{1}{r_p-r} - \frac{(\Omega r+w)^3}{8\pi r[u^2+(\Omega r+w)^2]^{\frac{3}{2}}} \ln\left|\frac{r_p-r}{R_p}\right| \quad (24)$$

$$\delta_v \equiv 0 \quad (25)$$

$$\delta_w \equiv -\frac{u}{\Omega r+w} \delta_u \quad (26)$$

where u and w are the inflow at r from the previous approximation, these singular parts can be integrated analytically in the usual principal value sense and the regular parts can be integrated by the generalized Gaussian scheme described previously. In these integrations, the derivative of Γ is found by differentiation of Eq. (22). The regular parts are determined numerically by subtracting the singular parts from the summation over all the blades of the influence functions.

The computer program can accommodate up to 108 elements for the trailing vortex sheet from any blade. Generally, we made our runs with 45 to 60 elements, between 20 and 35 of which were taken in the immediate neighborhood of the singularities to obtain adequate definition of the regular parts. The accuracy specified for the Gaussian integration was again $\pm$ 0.00005 of the tip rotational speed. This required 4 to 20 subdivisions between the hub and tip.

If the induced velocity off the blades and trailing vortex sheets is desired, the contribution from the trailing vortex sheets has no singular part, and so integration proceeds exactly as for the regular part.

Use of Main Computer Program

A total of 31 runs was made with the main computer program, 10 of which were for development purposes. These are summarized in Table 2 to show the specific propellers considered and pitch settings at the 0.7 radius, together with the purpose of the run. In the propeller designations, the digit in front (3 for all these particular propellers) is the number of blades, while the digits and letters within the parentheses refer to the blade design, see Appendix II.

TABLE 2

SUMMARY OF RUNS WITH MAIN COMPUTER PROGRAM

Run	Propeller		Purpose of Run
1-5	3(10188A2P2)	$\beta_{0.7R_p} = 10.0°$	Check out computer program by repeating first approximation to inflow using Pitchfork Model (Ref. 9, p. 17).
6,7	3(10188A2P2)	20.0°	As Runs 1-5 (Ref. 10, p. 16).
8,10	3(10188A2P2)	10.0°	Compute first approximations to inflow using Pitchfork Model with infinite roll-up times for two different sets of increment sizes in the marching scheme.
9,11,14	3(10188A2P2)	10.0°	Check out computer program for Continuous Deformation Model and compute first approximations to inflow using an initial wake hypothesis for two different numbers of steps at one set of increment sizes in the marching scheme.
12	3(10188A2P2)	20.0°	Compute first approximation to inflow using Pitchfork Model as in Runs 8, 10.
13	3(109654)	11.3°	Compute first approximation to inflow using the initial wake hypothesis.
15,16	3(109654)	11.3°	Compute second approximations to inflow using the initial wake hypothesis and two different sets of iteration factors K_u , K_v & K_w .

TABLE 2 - contd.

17	3(109652)	$\beta_{0.7R_p}$ = 10.0°	As Run 13.
18	3(109652)	14.0°	As Run 13.
19	3(109652)	16.0°	As Run 13.
20	3(109652)	10.0°	Compute second approximation to inflow using the initial wake hypothesis.
21	3(109652)	14.0°	As Run 20.
22	3(109652)	16.0°	As Run 20.
23,24	3(109652)	14.0°	Compute third approximations to inflow using the initial wake hypothesis and two different hub geometries.
25	3(109652)	10.0°	Compute third approximation to inflow using the initial wake hypothesis.
26	3(109652)	16.0°	As Run 25.
27	3(109654)	11.3°	As Run 25.
28	3(109652)	10.0°	Compute first approximation to inflow using a refined wake hypothesis.
29	3(13168A10P3)	14.0°	Compute first approximation to inflow using the refined wake hypothesis.
30	3(13168A10P3)	14.0°	As Run 29 for second approximation.
31	3(13168A10P3)	14.0°	As Run 29 for third approximation.

For the earlier runs, the FORTRAN 63 deck was used. Subsequently, a BINARY deck was cut once some confidence had been established. This saved about 6 minutes in compilation.

The running times for the BINARY deck varied from 15 to 40 minutes. The major part of this time was spent on the march along the trajectories, the remaining operations taking about 5 minutes in any run. Since the number of steps at the initial time increment was fixed, the variation in running time can be traced essentially to the number of steps required at the second time increment to reach the axial location for termination of the march. This depends only upon the axial component of velocity along the trajectory which reaches this termination point last.

Description of the wake hypotheses and other details, as well as the results of the runs, will be presented in the next chapter.

CHAPTER 3

THEORETICAL RESULTS

General

As summarized in Table 2, calculations were carried out for four propellers: the 3(10188A2P2), the 3(109654), the 3(109652) and the 3(13168A10P3). In this chapter we will present the specific orientation of these calculations for each of the propellers, the input data including the wake hypothesis used, the pertinent results and the intermediate conclusions reached. Comparison with test data, where appropriate, will be presented and discussed in Chapter 5.

3(10188A2P2) Propeller

The objectives of the calculations for the 3(10188A2P2) propeller were twofold: first, to check out the main computer program; and second, to compare the Pitchfork Model with the Continuous Deformation Model. Accordingly, no comparisons with test data were planned.

The choice of input was made as follows. The Pitchfork Model described earlier for finite roll-up times was rerun at both the 10.0° and 20.0° pitch settings (Ref. 9, p. 17; Ref. 10, p. 16). Runs were also made at these settings for infinite inboard and outboard roll-up times. The Continuous Deformation Model was run only at the 10.0° setting. As an initial wake hypothesis or approximation to the force-free condition of the wake, we assumed that the variation of the induced velocity along constant radii, regardless of the blade circulation, was given by the Generalized Actuator Disk theory (Ref. 14, pp. 21, 29). This variation was modified slightly by assuming that the wake reached its final, regular helical shape at a finite distance downstream, namely one and one-half radii, instead of an infinite distance. Thus, the wake could be calculated completely on a theoretical basis. The airfoil data for these calculations were found following the procedure of the C-W static strip analysis (Ref. 11, pp. 8 to 12, 19 to 21) with corrections to a tip speed of 650 feet per second. The zeroth approximations to the axial and tangential inflow components also were based on this analysis. Since it does not provide the radial component, we took for the Continuous

Deformation Model the finite roll-up time values with some smoothing of the distribution near the blade tip. The iteration factors in Eqs. (19) to (21) were all taken equal to one.

The resulting first approximations to the axial, radial and tangential inflow components are presented in Table 3, together with the zeroth, or initial, approximation. The Pitchfork Model results for finite roll-up times agreed well with the original results. The Continuous Deformation Model gave an axial component over the middle of the blade comparable to that of the Pitchfork Model with finite roll-up times. Both were greater than the zeroth approximation there but fell below it outboard of the 0.7 radial station with the Continuous Deformation Model, even leading to negative values near the tip. On the other hand, the infinite roll-up time values were considerably greater than all the others over the entire blade. Investigation of the contribution of the elements of the vortex sheet trailing inboard and outboard of the maximum of the blade circulation showed that this increase arose solely from the outboard vortex elements. That is, the axial velocity, and thus the pitch of these elements, was so low near the tip that the magnitude of their interference on the passing blades was extremely sensitive to their precise length. This trend with roll-up time was the same that was seen in our earlier studies (Ref. 9, p. 25). At the 20.0° setting on the other hand, the axial velocity and pitch were higher near the tip and the finite and infinite roll-up time results differed by less than 5% over the entire blade for all inflow components. The radial inflow components at 10.0° generally were consistent with the axial components throughout. There were only small differences in the tangential inflow components, lending further support to our previous observation (Ref. 9, pp. 10, 20) that the tangential velocity is a function only of Γ/r (cf. Ref. 14, p. 17).

These results showed that the main computer program worked successfully and that the envelopes of the trajectories of the elements of the trailing vortex sheets, as predicted by the initial wake hypothesis, were physically reasonable. To investigate this hypothesis in more detail, we proceeded to the 3(109654) propeller.

3(109654) Propeller

The objectives of the calculations for the 3(109654) propeller were also twofold: first, to iterate to a solution of Eqs. (13)

TABLE 3

FIRST APPROXIMATIONS TO INFLOW
VARIOUS WAKE MODELS

3(10188A2P2) Propeller
$\beta_{0.7R_p} = 10.0°$

	$u/\Omega R_p$				$v/\Omega R_p$		
r/R_p	0^{th}	P_f	P_∞	CD	0^{th}	P_f	P_∞
0.2	0.0708	0.0759	0.1405	0.0394	-0.0042	-0.0042	-0.00
0.3	0.0937	0.1040	0.1691	0.0900	-0.0126	-0.0126	-0.02
0.4	0.1044	0.1307	0.1956	0.1284	-0.0227	-0.0227	-0.03
0.5	0.1017	0.1291	0.1943	0.1274	-0.0330	-0.0330	-0.05
0.6	0.0965	0.1275	0.1926	0.1209	-0.0427	-0.0427	-0.06
0.7	0.0848	0.1076	0.1717	0.0913	-0.0511	-0.0511	-0.08
0.8	0.0638	0.0624	0.1233	0.0323	-0.0571	-0.0571	-0.09
0.9	0.0405	0.0266	0.0791	-0.0140	-0.0615	-0.0606	-0.11
0.95	0.0247	0.0081	0.0505	-0.0273	-0.0632	-0.0619	-0.12
0.975	0.0156	0.0023	0.0372	-0.0287	-0.0640	-0.0649	-0.12

0^{th} - Zeroth Approximation
P_f - Pitchfork Model, Finite Roll-Up Times
P_∞ - Pitchfork Model, Infinite Roll-Up Times
CD - Continuous Deformation Model, Initial Wake Hypothesis

TABLE 3

FIRST APPROXIMATIONS TO INFLOW COMPONENTS
VARIOUS WAKE MODELS

3(10188A2P2) Propeller
$\beta_{0.7R_p} = 10.0°$

	$v/\Omega R_p$				$w/\Omega R_p$			
	0^{th}	P_f	P_∞	CD	0^{th}	P_f	P_∞	CD
94	-0.0042	-0.0042	-0.0099	0.0200	-0.0293	-0.0240	-0.0283	-0.0305
00	-0.0126	-0.0126	-0.0225	0.0020	-0.0329	-0.0396	-0.0422	-0.0406
84	-0.0227	-0.0227	-0.0365	-0.0179	-0.0294	-0.0475	-0.0489	-0.0432
74	-0.0330	-0.0330	-0.0516	-0.0368	-0.0216	-0.0369	-0.0377	-0.0338
09	-0.0427	-0.0427	-0.0674	-0.0523	-0.0159	-0.0293	-0.0299	-0.0259
13	-0.0511	-0.0511	-0.0835	-0.0618	-0.0104	-0.0183	-0.0187	-0.0160
13	-0.0571	-0.0571	-0.0994	-0.0620	-0.0051	-0.0065	-0.0067	-0.0063
10	-0.0615	-0.0606	-0.1153	-0.0448	-0.0018	-0.0013	-0.0013	-0.0008
13	-0.0632	-0.0619	-0.1224	-0.0333	-0.0006	-0.0002	0.0001	0.0002
17	-0.0640	-0.0649	-0.1264	-0.0296	-0.0002	-0.0000	0.0005	0.0004

ke Hypothesis

B

and (19) to (21) using the initial wake hypothesis; and second, to compare the resulting performance prediction with test data, at least in a preliminary fashion.

For input, a pitch setting of 11.3° was chosen and the airfoil data were found as for the 3(10188A2P2) propeller, here corrected to a tip speed of 1002 feet per second. The zeroth approximation to the axial inflow component was calculated as before, while $-N\Gamma/4\pi r$ was used for the tangential inflow once the blade circulation had been determined. The zeroth approximation to the radial velocity component was guessed so that the trajectory envelopes were similar to those for the 3(10188A2P2) propeller. First and second approximations were computed with the axial and radial iteration factors equal to one and the successive tangential components found as for the zeroth. Also first, second and third approximations were computed with all three iteration factors equal to one-half. The third approximation was computed after the calculations for the 3(109652) propeller and involved a different treatment of the hub geometry that will be discussed in the next section.

The zeroth approximation to the axial inflow component, the first and second approximations with the iteration factors equal to one, and the first, second and third approximations with the factors equal to one-half are given in Table 4 . The first approximation to the axial inflow with the factors equal to one behaved like the corresponding 3(10188A2P2) calculation, but the second approximation computed from it had a physically unreasonable character which prohibited continuation of the iteration. This character can be explained by separate examination of the contributions to the axial inflow from the singular and regular parts of the influence functions. Since Ωr dominates u and w, the strength of the Cauchy singularity in Eq. (24) does not vary greatly over the blade. While the strength of the logarithmic singularity does vary considerably, its total contribution is much smaller than that of the Cauchy singularity (Ref. 10, p. 23). Therefore the singular axial inflow contribution depends primarily upon the trailing vortex sheet strength. In the first approximation there was a heavy concentration of trailing vorticity outboard of the 0.9 radial station. This led to the rapid increase in the singular contribution to the axial inflow just inboard of the tip. The same effect was noted in our earlier calculations with the Pitchfork Model (Ref. 10, p. 22). On the other hand, the regular contribution to the axial inflow is a function of the detailed shape of the trajectories, as

TABLE 4

SUCCESSIVE APPROXIMATIONS TO AXIAL INFLOW COMPONENT $u/\Omega R_p$
INITIAL WAKE HYPOTHESIS

3(109654) Propeller
$\beta_{0.7R_p} = 11.3°$

		K_u & K_v = 1		K_u , K_v & K_w = ½		
r/r_p	0^{th}	1^{st}	2^{nd}	1^{st}	2^{nd}	3^{rd}
0.2	0.0387	-0.0025	0.0803	0.0170	0.0255	-0.0198
0.3	0.0755	0.0635	0.0681	0.0695	0.0645	0.0659
0.4	0.0832	0.0856	0.1017	0.0844	0.0862	0.0783
0.5	0.0863	0.0972	0.1145	0.0918	0.0952	0.0934
0.6	0.0869	0.0989	0.1264	0.0929	0.0986	0.0949
0.7	0.0858	0.0958	0.1264	0.0908	0.0961	0.0928
0.8	0.0818	0.0762	0.1354	0.0790	0.0855	0.0818
0.9	0.0704	0.0366	0.2086	0.0535	0.0519	0.0582
0.95	0.0612	0.0130	-0.0475	0.0371	0.0366	0.0572
0.975	0.0510	-0.0001	0.0712	0.0255	0.0460	-0.0009

well as of their strength. Here, as a result of moving ahead of the propeller initially, the contracting trailing vortex elements passed very close to the next blade at a reduced radius; e.g., the vortex element trailing from the tip passed 0.012 radii behind the next blade at the 0.923 radial station. The strong interference that resulted was observed in the regular contribution to the axial inflow. It, too, had the behavior associated with a concentration of vorticity, which now, however, was just inboard of the 0.923 station. Namely, there was a maximum in the regular contribution at about 0.90, a zero at about 0.93, and a minimum (which is negative) at about 0.95, outboard of which it increased. Summing these singular and regular contributions then gave the unusual character of the total axial velocity distribution. In order to provide a convergent iteration it was necessary to consider different iteration factors. We chose one-half, recalculated the first and second approximations accordingly, and obtained a convergent trend. The radial inflow in all approximations varied with the axial component in a way so that overall there were only small adjustments in the trajectory envelopes from step to step. The tangential inflow correlated with Γ/r as before.

We gained considerable insight into the question of convergence of the iteration from a simplified theory which we derived for static propellers. This is an adaptation of the Generalized Actuator Disk theory along lines also put forth independently by M. Iwasaki (Refs. 15 and 16). Basically only the radial variation of the mean, or θ-average, axial inflow is considered and all trailing vortex distortion is neglected. The system reduces accordingly to a single transcendental equation which is equivalent to Eq. (9) but exhibits complete independence of the blade sections. To solve this equation, we rewrote it in the form of Eq. (19) and iterated as in our complete analysis. We found divergence if the iteration factor were one, and convergence if it were one-half. The exact conditions for convergence (Ref. 23, pp. 184 to 187, for example) confirmed these results. Although our full system of equations is more complicated and has many features which are different, still the simpler system provided understanding and guidelines at least for choosing the iteration factors for convergence.

The principal conclusion of the first two approximations with iteration factors of one-half and one was that the former value led towards a convergent iteration. Comparison with experiment at this single pitch setting was inconclusive so further calculations were undertaken for the 3(109652) propeller.

3(109652) Propeller

The objectives of the calculations for the 3(109652) propeller were threefold: first, to predict the performance over a broad range of pitch settings, following the previous calculations; second, to compare the results with test data; and third, to refine the wake hypothesis as necessary.

For input, pitch settings of 10.0°, 14.0° and 16.0° were chosen for the initial wake hypothesis and the 10.0° setting for the refined wake hypothesis. This refined hypothesis or approximation to the force-free condition of the wake was identical to the initial hypothesis inboard of the 0.5 radial station. Outboard, the variation of the axial induced velocity component from the Generalized Actuator Disk theory was applied along streamlines rather than along constant radii. The variation of the radial induced velocity component was then fixed by assuming that both the initial and refined wake hypotheses should give the same trajectory envelopes. For the tangential component the refined hypothesis was assumed identical with the initial hypothesis, since w is small compared to Ωr . The airfoil data were determined as before and were corrected to a tip speed of 785 feet per second. The zeroth approximations to the axial and tangential inflow components were also found by the earlier strip analysis. Three different distributions of radial inflow were assumed at each pitch setting and their trajectories were calculated by means of the short trajectory program. From these, the most promising distribution was selected, based upon experience. All three iteration factors were one-half and the first two approximations were computed for all three settings. At the 14.0° setting, third approximations were calculated with the hub geometry treated more like a wing tip, as in the first two approximations, and also, more like a wing root, see Appendix II. This latter treatment was continued not only for the third approximations of this propeller at the 10.0° and 16.0° settings, but for the third approximation of the 3(109654) propeller at 11.3° as well.

In Table 5 are presented the zeroth, first, second and third approximations to all three inflow components at 10.0°, together with the corresponding values from the refined wake hypothesis which used the second approximation as input. Iteration behaved similarly at all three pitch settings and converged sufficiently well to the accuracy required for comparison of the performance predictions with experiment. The first and third approximations to the axial inflow distribution were very close, both in magnitude and shape, while the

TABLE

SUCCESSIVE APPROXIMATIONS
INITIAL AND REFINED

$3(109652)$ P
$\beta_{0.7R_p}$ =

	$u/\Omega R_p$							v
r/R_p	0^{th}	1^{st}	2^{nd}	3^{rd}	RWH	0^{th}	1^{st}	
0.2	0.0491	0.0305	0.0265	0.0220	0.0781	0.0185	0.0283	0
0.3	0.0722	0.0626	0.0602	0.0608	0.1166	0.0060	0.0204	0
0.4	0.0857	0.0936	0.0950	0.0914	0.1464	-0.0059	0.0026	0
0.5	0.0863	0.0966	0.1002	0.0959	0.1497	-0.0168	-0.0148	-0
0.6	0.0836	0.0907	0.0962	0.0922	0.1435	-0.0278	-0.0300	-0.
0.7	0.0823	0.0874	0.0926	0.0941	0.1399	-0.0380	-0.0425	-0.
0.8	0.0750	0.0696	0.0823	0.0678	0.1012	-0.0477	-0.0514	-0.
0.9	0.0642	0.0500	0.0363	0.0511	0.0564	-0.0545	-0.0515	-0.
0.95	0.0488	0.0220	0.0290	0.0207	0.0146	-0.0572	-0.0485	-0.
0.975	0.0391	0.0157	0.0254	0.0104	0.0032	-0.0580	-0.0469	-0.

0^{th} Zeroth Approximation
1^{st} First Approximation, Initial Wake Hypothesis
2^{nd} Second Approximation, Initial Wake Hypothesis
3^{rd} Third Approximation, Initial Wake Hypothesis
RWH First Approximation, Refined Wake Hypothesis

TABLE 5

ATIONS TO INFLOW COMPONENTS
EFINED WAKE HYPOTHESIS

652) Propeller
.7R_p = 10.0°

	$v/\Omega R_p$			$w/\Omega R_p$				
	2^{nd}	3^{rd}	RWH	0^{th}	1^{st}	2^{nd}	3^{rd}	RWH
3	0.0325	0.0322	0.0242	-0.0129	-0.0150	-0.0150	-0.0147	-0.0147
4	0.0320	0.0270	0.0145	-0.0186	-0.0221	-0.0230	-0.0236	-0.0236
6	0.0098	0.0106	-0.0069	-0.0193	-0.0253	-0.0266	-0.0274	-0.0274
8	-0.0110	-0.0092	-0.0326	-0.0154	-0.0208	-0.0224	-0.0228	-0.0228
0	-0.0284	-0.0260	-0.0567	-0.0119	-0.0160	-0.0176	-0.0179	-0.0179
2	-0.0437	-0.0418	-0.0814	-0.0098	-0.0130	-0.0142	-0.0150	-0.0150
4	-0.0573	-0.0588	-0.1090	-0.0071	-0.0086	-0.0104	-0.0096	-0.0096
5	-0.0654	-0.0638	-0.1145	-0.0046	-0.0046	-0.0046	-0.0054	-0.0057
5	-0.0515	-0.0461	-0.0825	-0.0025	-0.0016	-0.0019	-0.0022	-0.0022
9	-0.0452	-0.0402	-0.0722	-0.0016	-0.0010	-0.0012	-0.0011	-0.0011

B

second approximation, though not greatly different in magnitude, was distinctly different in shape. This trend was observed for the 3(109654) propeller too. As can be seen, the axial inflow distribution fell off near the tip at 10.0°; however, at 14.0° and 16.0° the axial inflow distributions remained high at the tip, and both were of similar shape. The radial inflow distributions were remarkably similar in shape and magnitude for all three pitch settings, while the tangential inflow again correlated well with Γ/r . In Fig. 4, the third approximations to the inflow components are plotted for the initial and refined wake hypotheses. The large differences are clarified by Fig. 5 which shows the projections for the respective trajectories of the tip element of one vortex sheet. For the refined hypothesis, we see that the "pitch" is much lower, and so, the axial and radial inflow much larger. This is analogous to the differences between the inflow in the Pitchfork Model for infinite and finite roll-up times, i.e., a finite roll-up time provides an effective pitch increase. The change in hub geometry had only a local effect on the inflow. Outboard of the 0.5 station the difference was less than 3% .

The first conclusion reached was that the refined wake hypothesis should be used for subsequent calculations. This was based primarily on comparisons between theory and experiment which will be discussed in Chapter 5. Although the envelopes of the trajectories are predicted quite well by the initial wake hypothesis, their "pitch", which is critical, is described much better by the refined wake hypothesis. We also concluded that a different choice for the iteration factors was necessary. Study indicated that further improvement could be gained by choosing one-quarter for these factors.

3(13168A10P3) Propeller

The objectives of the calculations for the 3(13168A10P3) propeller were twofold: first, to predict the performance at one pitch setting using the refined wake hypothesis; and second, to compare the results with test data.

For input, a pitch setting of 14.0° was chosen. The airfoil data were applied in a slightly different fashion from that of the earlier static strip analysis. Namely, the basic section data (Ref. 7) were read at the Mach number and Reynolds number appropriate to the tip speed of 750 feet per second. Although the data were extended as before (Ref. 11, pp. 8, 9)

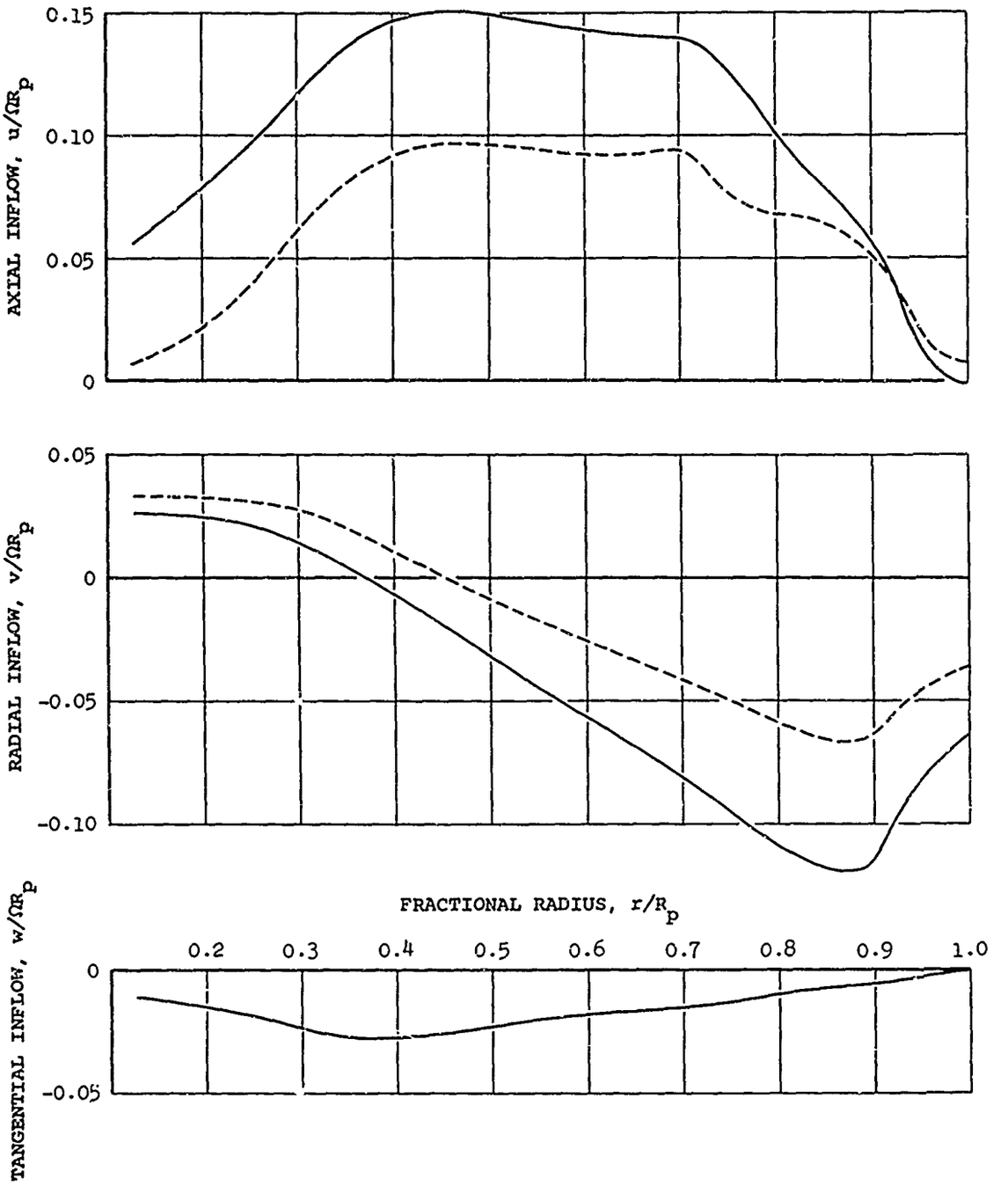

Figure 4. Inflow Components for Initial (--) and Refined (—) Wake Hypotheses. 3(109652) Propeller, $\beta_{0.7R_p} = 10.0°$.

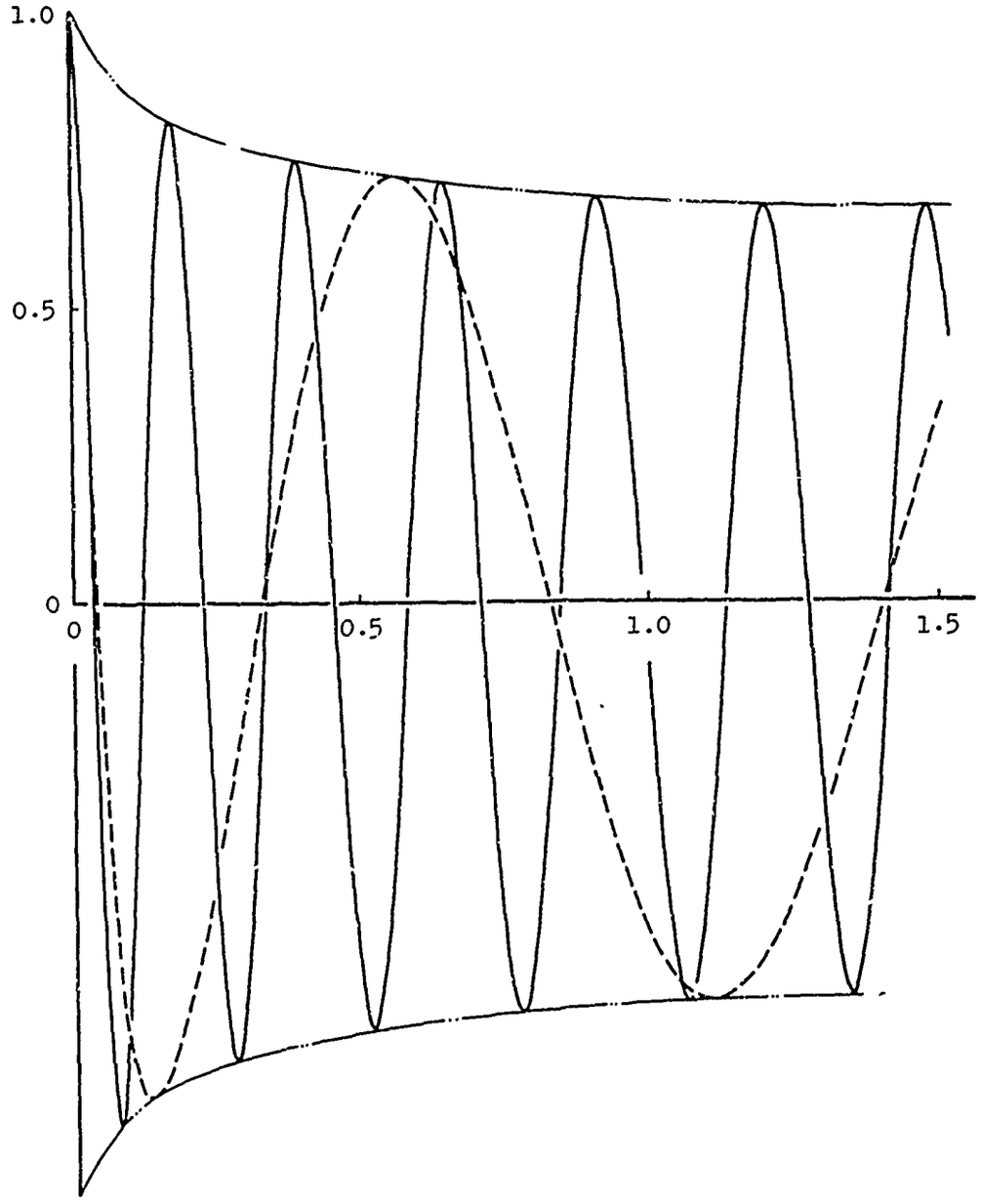

Figure 5. Trajectory Projection of Vortex Sheet Element from Tip. Initial (--) and Refined (—) Wake Hypotheses, 3(109652) Propeller, $\beta_{0.7R_p} = 10.0°$.

to high angles of attack, the factor of 1.1 in the drag coefficient (Ref. 11, p. 21) was omitted. We determined the zeroth approximation to the axial inflow component as for the other propellers and used $-N\Gamma/4\pi r$ for the tangential component once the blade circulation was known. Again, three different distributions of radial velocity were tried and the one with the most promising trajectories was selected. First, second and third approximations were calculated with the axial and radial iteration factors equal to one-quarter, and the successive tangential components were found as for the zeroth.

In Table 6 are presented the zeroth, first, second and third approximations to all three inflow components. The axial inflow changed smoothly from step to step. Inboard near the hub and outboard of the 0.8 radial station the iteration converged. Over the middle of the blade, the convergence trend was inconclusive as far as the iteration was carried out. This behavior was distinctly different from our previous iterations. The radial inflow component became steadily more negative, which led to more realistic trajectory envelopes inboard. As found throughout, good correlation with Γ/r was observed for the tangential inflow.

The main conclusion which we drew from these calculations was that the convergence properties of the iteration with the refined wake hypothesis and iteration factors of one-quarter are different. It appears that one or possibly two further approximations are required to achieve complete convergence over the whole blade.

TABLE 6

SUCCESSIVE APPROXIMATIONS TO INFLO
REFINED WAKE HYPOTHESI

3(13168A10P3) Propelle
$\beta_{0.7R_p} = 14.0°$

	$u/\Omega R_p$				$v/\Omega R_p$		
r/R_p	0^{th}	1^{st}	2^{nd}	3^{rd}	0^{th}	1^{st}	$2^{}$
0.2	0.0759	0.0755	0.0755	0.0798	0.0263	0.0227	0.0
0.3	0.0958	0.0982	0.1052	0.1137	0.0197	0.0156	0.0
0.4	0.1072	0.1137	0.1214	0.1303	0.0080	0.0024	-0.0
0.5	0.1127	0.1246	0.1298	0.1396	-0.0085	-0.0150	-0.0
0.6	0.1119	0.1233	0.1356	0.1406	-0.0251	-0.0327	-0.0
0.7	0.1035	0.1146	0.1170	0.1264	-0.0389	-0.0474	-0.0
0.8	0.0859	0.0849	0.0880	0.0898	-0.0483	-0.0572	-0.0
0.9	0.0657	0.0560	0.0505	0.0497	-0.0530	-0.0590	-0.0
0.95	0.0562	0.0432	0.0378	0.0311	-0.0539	-0.0566	-0.0
0.975	0.0535	0.0405	0.0336	0.0316	-0.0540	-0.0553	-0.05

0^{th} - Zeroth Approximation
1^{st} - First Approximation
2^{nd} - Second Approximation
3^{rd} - Third Approximation

TABLE 6

IVE APPROXIMATIONS TO INFLOW COMPONENTS
REFINED WAKE HYPOTHESIS

3(13168A10P3) Propeller
$\beta_{0.7R_p} = 14.0°$

$v/\Omega R_p$				$w/\Omega R_p$			
0th	1st	2nd	3rd	0th	1st	2nd	3rd
0.0263	0.0227	0.0193	0.0149	-0.0391	-0.0377	-0.0387	-0.0366
0.0197	0.0156	0.0116	0.0058	-0.0431	-0.0372	-0.0350	-0.0337
0.0080	0.0024	-0.0032	-0.0095	-0.0415	-0.0356	-0.0331	-0.0317
-0.0085	-0.0150	-0.0212	-0.0280	-0.0382	-0.0306	-0.0290	-0.0269
-0.0251	-0.0327	-0.0393	-0.0470	-0.0318	-0.0276	-0.0233	-0.0227
-0.0389	-0.0474	-0.0554	-0.0648	-0.0243	-0.0190	-0.0186	-0.0163
-0.0483	-0.0572	-0.0672	-0.0797	-0.0144	-0.0129	-0.0122	-0.0119
-0.0530	-0.0590	-0.0678	-0.0796	-0.0069	-0.0075	-0.0083	-0.0083
-0.0539	-0.0566	-0.0614	-0.0673	-0.0040	-0.0050	-0.0055	-0.0062
-0.0540	-0.0553	-0.0580	-0.0622	-0.0025	-0.0034	-0.0040	-0.0042

B

CHAPTER 4

TEST MEASUREMENTS

General

It is desirable to describe some of the experimental investigations made in support of the analysis. These test data proved useful not only to guide the theory toward its final form, but to assess the calculated predictions.

The available test data fall into two categories. The first is propeller wake velocity distributions along a blade radius measured with a hot-film anemometer. The second category is overall propeller performance presented in nondimensional form as thrust coefficient, pitch setting and figure of merit, all as a function of the power coefficient.

The three propellers that were tested are the 3(109654), the 3(109652) and the 3(13168A10P3). Blade characteristics for these propellers are shown in Appendix II . To date, wake surveys have only been made behind the 3(109654) and 3(109652) propellers.

All of the measured data for the 3(109654), 3(109652) and 3(13168A10P3) propellers incorporated in this report were obtained on the Curtiss Static Test Rig, which was placed in operation 3 years ago.

Description of Curtiss Static Test Rig

The rig is mounted out of doors on a concrete slab, see Fig. 6 . The propeller is cantilevered well away from the R-3350 engine mounting to minimize wake blockage and interference effects. It is capable of testing propellers up to 18 feet in diameter, supplying as much as 2500 horsepower.

A few feet upstream of the engine output shaft, the shaft is broken to include a Baldwin-Lima-Hamilton A-160 Torque Cell as shown in the schematic of Fig. 7 . Proceeding along the shaft toward the propeller, the shaft is again broken to contain a metal diaphragm. The purpose of the diaphragm is to preload the tapered roller thrust bearings so as to eliminate unwanted deflections of the bearings as well as any thermal

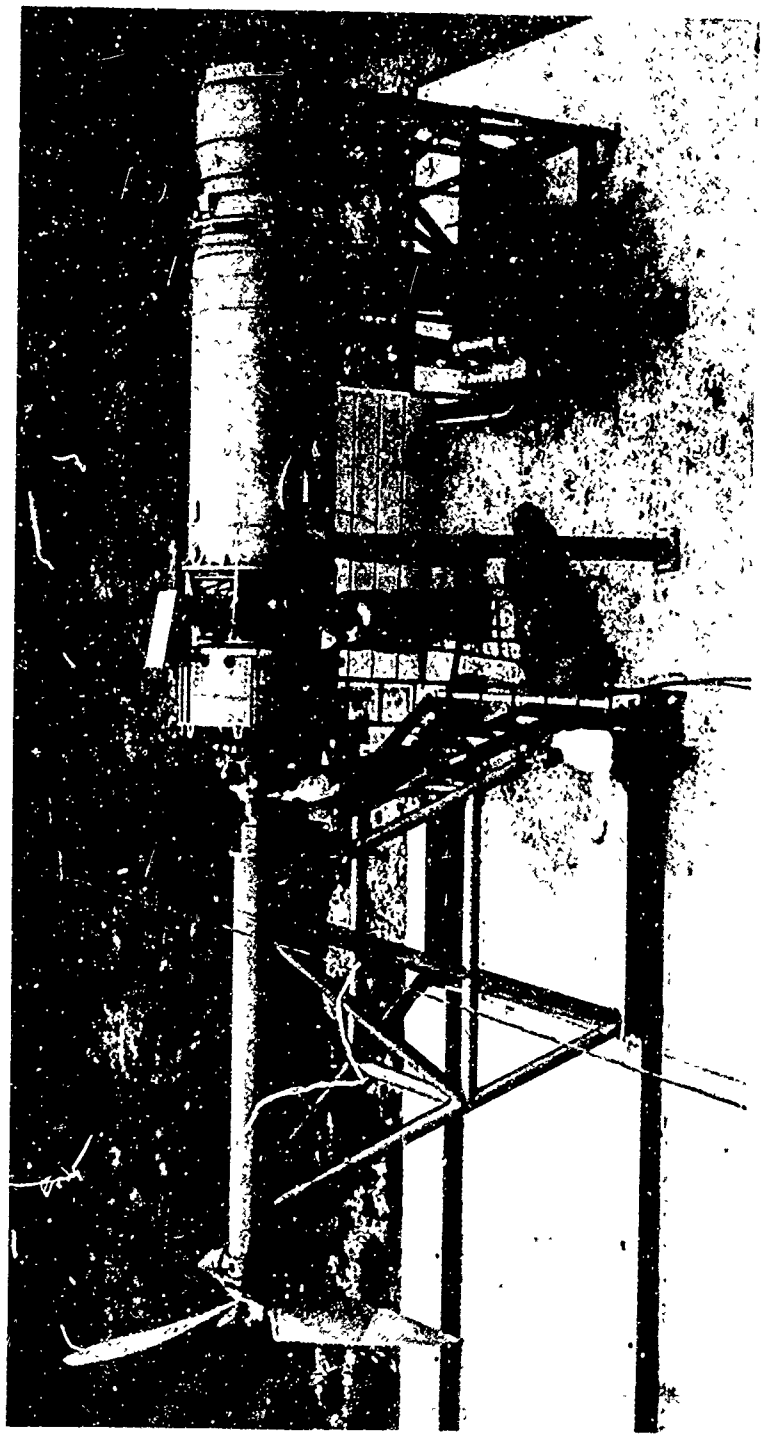

Figure 6. Curtiss Static Test Rig.

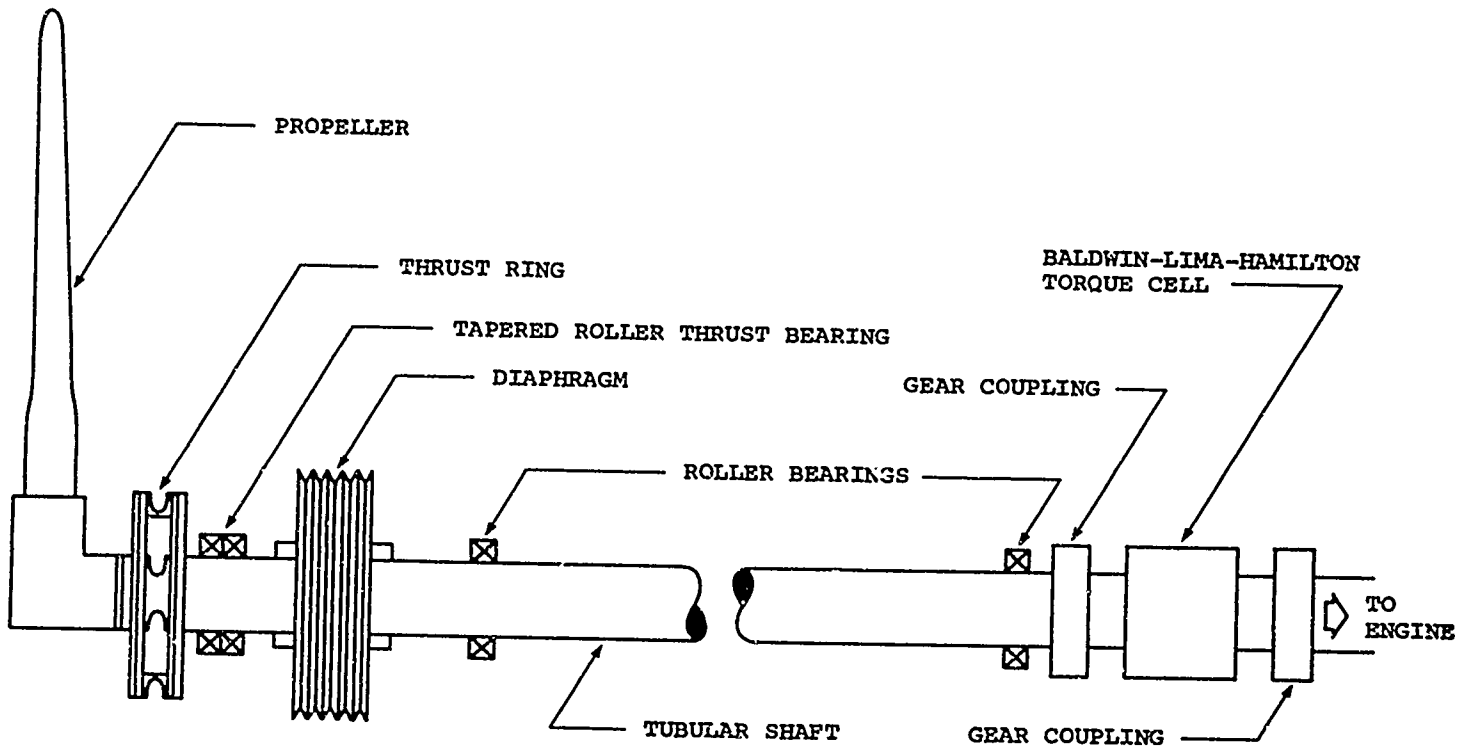

Figure 7. Schematic of Curtiss Static Test Rig.

growth of the shaft. This isolates the thrust load at the strain gaged, four-leg thrust ring which is located just aft of the propeller. The gage installation is designed to be insensitive to changes in temperature caused by frictional energy.

Thrust, torque, propeller RPM and wind velocity signals are read out on four channels of a DYMEC Digital Data Acquisition System. Thrust and torque signals taken from the thrust ring and torque cell are scanned and printed on tape. Readout accuracy is on the order of 0.1% . The propeller RPM is measured with a magnetic pickup directly on the propeller shaft and is also printed out. Because of the effect of wind on the performance of a static propeller, wind velocity measured with a cup anemometer is also monitored. Useful data are not obtainable when the steady velocity is above 3 miles per hour. The total scanning time for a cycle of all four channels is a little over 1 second.

The DYMEC system's output print-out is in volts, making it necessary to calibrate the system. The thrust is calibrated immediately after each run with the use of a deadweight. The deadweight of 6100 pounds is passed over a pulley and hooked to the propeller hub. A hydraulic ram raises the weight off the ground. The entire calibration takes about 2 minutes. The torque cell is calibrated periodically by the use of levers and arms and requires half a day for completion.

Repeat runs on various propellers have shown excellent agreement, and the data are felt to have better than $\pm$ 2% accuracy.

Description of Hot-Film Anemometer

It is difficult to obtain accurate propeller wake surveys since both the magnitude and the direction of the local velocity vector must be found. In addition, the instrumentation must be capable of measuring the rapid velocity variations with time (as seen here in space-fixed coordinates in contrast to the steady flow seen in propeller-fixed coordinates), that are associated with the finite blade number. This requires a very short response time.

The instrument used is the Lintronic Model 40W Linear Constant Temperature Hot-Film Anemometer. It is similar in principle to the hot-wire anemometer. That is, a thin pre-heated platinum element, which is extremely sensitive to

temperature differentials caused by variations in airflow, is mounted on a Pyrex glass wedge. The hot-film anemometer is rugged and maintains stability in physical characteristics for extended periods of time, yielding good signal to noise ratio and very high frequency response. Most important, it has been designed to yield a linear variation of velocity with electrical signal so that a quick calibration at one point is sufficient. A complete description including circuit diagrams can be found in the operating manual (Ref. 2).

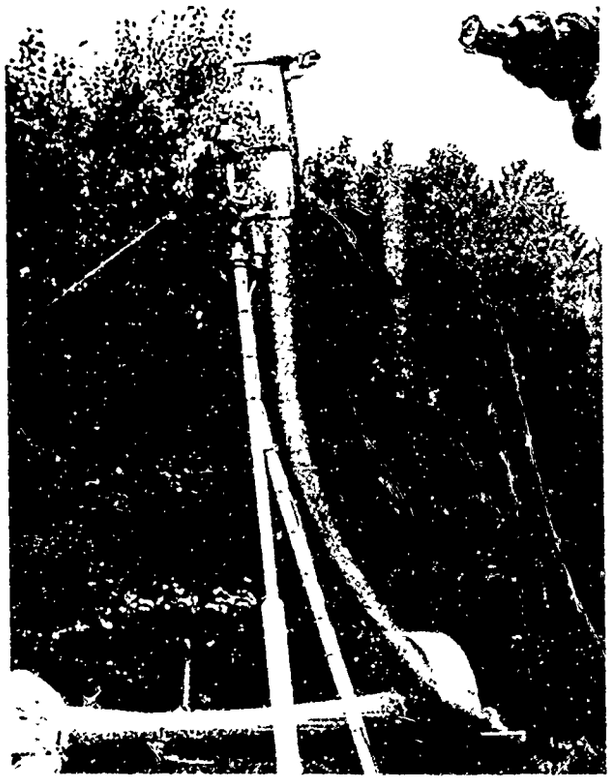

Figure 8. Hot-Film Anemometer Probe.

The test probe is mounted on a boom that can be positioned at any distance aft of the disk and at any station along the blade radius. The boom is shown in the photograph of Fig. 8. By remote control the probe can be rotated about its tip and also about its axis of symmetry. These degrees of freedom

enable the element of the probe to be positioned perpendicular to the resultant velocity vector, much in the same way a total pressure tap opening must be aligned to the flow to get a meaningful result.

The test probe is calibrated by dropping the probe into a small test section upstream of a blower. This test section is positioned so that as a propeller wake is being surveyed, the probe can be immediately dropped into the test section for a check calibration in a matter of seconds. This small wind chamber-blower arrangement is shown at the bottom of the photograph of Fig. 8 . In the wind chamber, uniform flows up to 220 feet per second can be maintained at the test section. By throttling the flow, while noting probe voltage, a calibration of voltage versus velocity is obtained.

The test procedure is as follows. The orientation of the probe is adjusted until the maximum signal voltage is obtained. Then the space coordinates, in this case three angles, are recorded together with the probe voltage which is highly damped to read an average value. An oscillograph records the unsteady portion of the velocity field. This procedure of maximizing the average velocity component simplifies considerably the test procedure. It is not necessary to seek a maximum unsteady velocity, since the unsteady portion of the velocity is less than 10% of the resultant. Limited tests have shown that the average-to-peak-velocity ratio does not vary with small excursions of the probe alignment.

A curve showing average axial velocity measurements for the 3(109652) propeller is presented in Fig. 9 . The probe was positioned 10 inches behind the trailing edge of the propeller blade, giving a minimum safe clearance of a few inches between the propeller blade and the probe support structure. An example of the data taken from the oscillograph records is shown in Fig. 10 . Average-to-peak-velocity ratio is plotted versus blade radius. These data were used to convert the data of Fig. 9 to compare with the inflow at the blade predicted by the theory. Repeatability of valid velocity data is within $\pm$ 3% in the axial velocity direction.

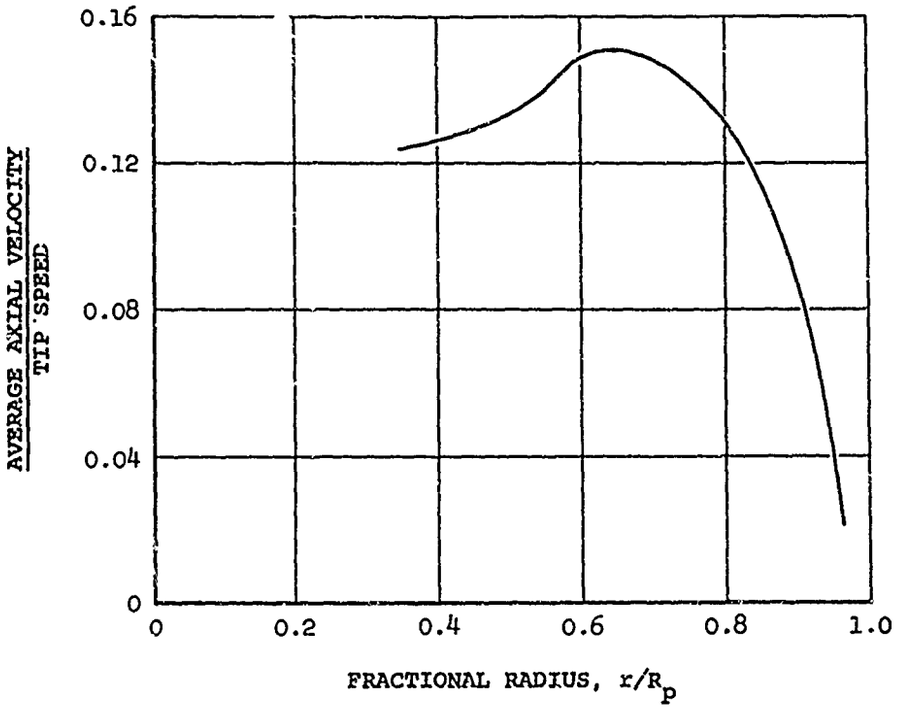

Figure 9. Axial Wake Velocity Test Data. (Measured 10" Aft of Propeller), 3(109652) Propeller, T = 4870 lb, P = 865 hp, ΩR_p = 785 fps.

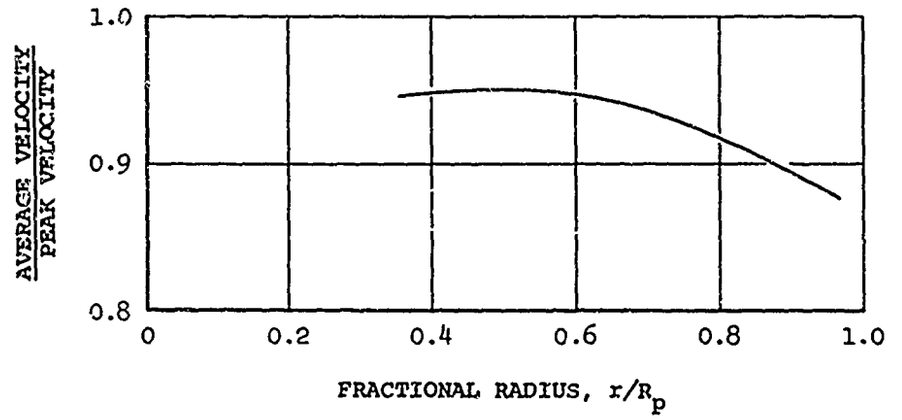

Figure 10. Test Data for Average-to-Peak-Velocity Ratio. (Measured 10" Aft of Propeller), 3(109652) Propeller, T = 4870 lb, P = 865 hp, ΩR_p = 785 fps.

CHAPTER 5

COMPARISON OF THEORY WITH TEST DATA

Scope

As indicated earlier, the theoretical calculations for the 3(10188A2P2) propeller were for check-out and preliminary evaluation purposes only and will not be compared with test data at all. Since calculations for the 3(109654) propeller were also primarily for theoretical purposes, their comparison will be limited in extent. The principal comparisons which we will make are for the 3(109652, and 3(13168A10P3) propellers.

3(109654) Propeller

The third approximation using the initial wake hypothesis with the iteration factors equal to one-half is chosen as the final theoretical result for the 3(109654) propeller at the 11.3° pitch setting.

Comparison of the axial inflow over the middle portion of the blade where data are available indicates that the theoretical values are on the order of 65% of the measured values. If the first or second approximations are used instead, these results are varied by about 10% .

The performance predictions fall roughly 7% below the measured power coefficient, 3% above the measured thrust coefficient and 10% above the measured figure of merit. Again the maximum variations in these performance predictions in the iteration are 1%, 4%, and 3%, respectively.

3(109652) Propeller

The third approximation using the initial wake hypothesis with the iteration factors equal to one-half is chosen as the final theoretical result for the 3(109652) propeller at the 10.0°, 14.0° and 16.0° pitch settings. For the preliminary evaluation of the refined wake hypothesis, the single approximation at the 10.0° setting is considered.

Comparison of the theoretical and measured distributions of the axial inflow at the 14.0° pitch setting is presented in Fig. 11 . The measured values were extrapolated to the propeller blades from the data measurements 10 inches

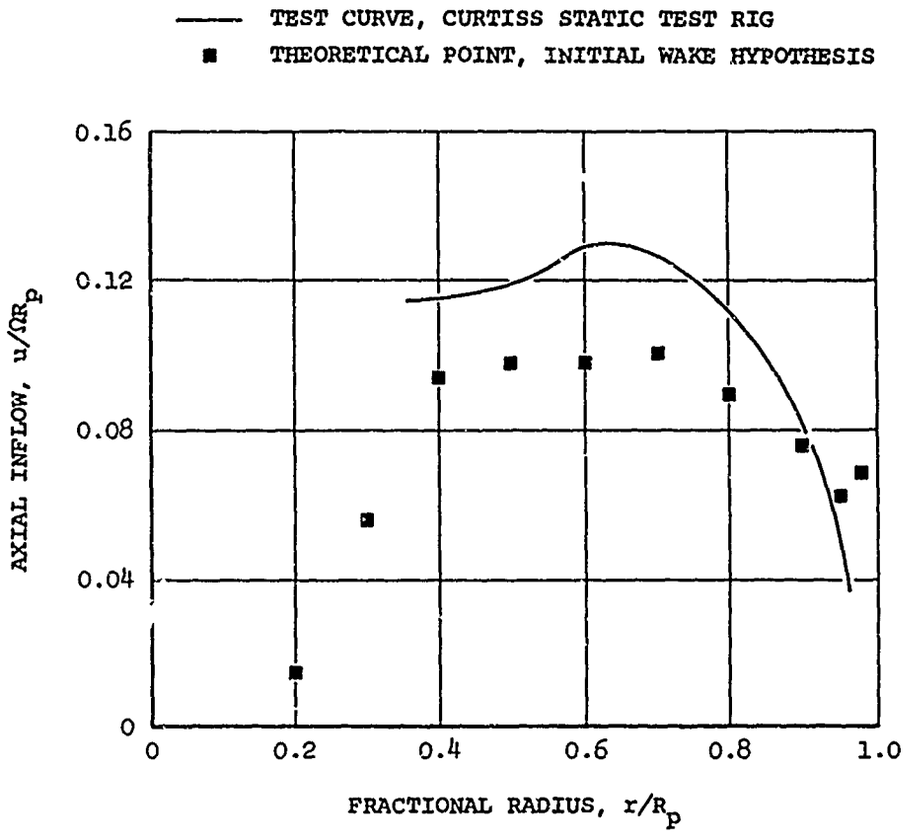

Figure 11. Axial Inflow Comparison of Theory (Initial Wake Hypothesis) with Test Data. 3(109652) Propeller, $\beta_{0.7R_p} = 14.0°$, $\Omega R_p = 785$ fps.

behind the propeller, see Figs. 9 and 10 . The initial wake hypothesis was used, since at this distance downstream it does not differ much from the refined wake hypothesis. As for the 3(109654) propeller the theoretical results fall generally below the measured values but not by as much. At the 0.7 station, the corresponding error in α is about 20% . Again, the maximum variation of axial inflow in the iteration is approximately 10% .

The performance predictions over the range of pitch settings are given in Figs. 12 to 14 . The overall comparison based upon the initial wake hypothesis is unfavorable, generally the predictions being worst at the 10.0° pitch setting. Most disturbing, the entire qualitative shape of the figure of merit versus power coefficient curve is incorrect. Maximum variations in the iteration of the power and thrust coefficients and figure of merit are about 2%, 4% and 6%, respectively, at 10.0°; 2%, 2% and 3% at 14.0°; and 3%, 3% and 1% at 16.0° . The effect at 14.0° of the different treatment of the hub geometry was much less than 1% .

The performance predictions of the refined wake hypothesis are also presented in Figs. 12 to 14 for iteration factors of both one-quarter and one-half. With either, the trend is very encouraging. Furthermore, study indicates that the refinement would also improve the performance prediction at the 14.0° and 16.0° settings. These results based on this single approximation should not be construed as a final answer but are subject to iteration.

3(13168A10P3) Propeller

The third approximation using the refined wake hypothesis and iteration factors equal to one-quarter is chosen as the final theoretical result for the 3(13168A10P3) propeller at the 14.0° pitch setting.

Comparisons of the performance predictions with the test data in Figs. 15 to 17 are excellent. With regard to convergence, the predictions generally improved with each step in the iteration, moving monotonically from the zeroth approximation to the third approximation. The respective values found for the thrust coefficient from the zeroth, first, second and third approximations were 0.158, 0.151, 0.145 and 0.140 . For the power coefficient, the corresponding values were 0.0638, 0.0612, 0.0587 and 0.0576 ; and for the figure of merit, they were 78.5%, 76.5%, 75.0% and 72.6% . Consequently, we again see that further approximations are required, as noted earlier.

Summary of Performance Comparisons

Table 7 gives an overall picture of the performance comparisons for the 3(109654), 3(109652) and 3(13168A10P3) propellers.

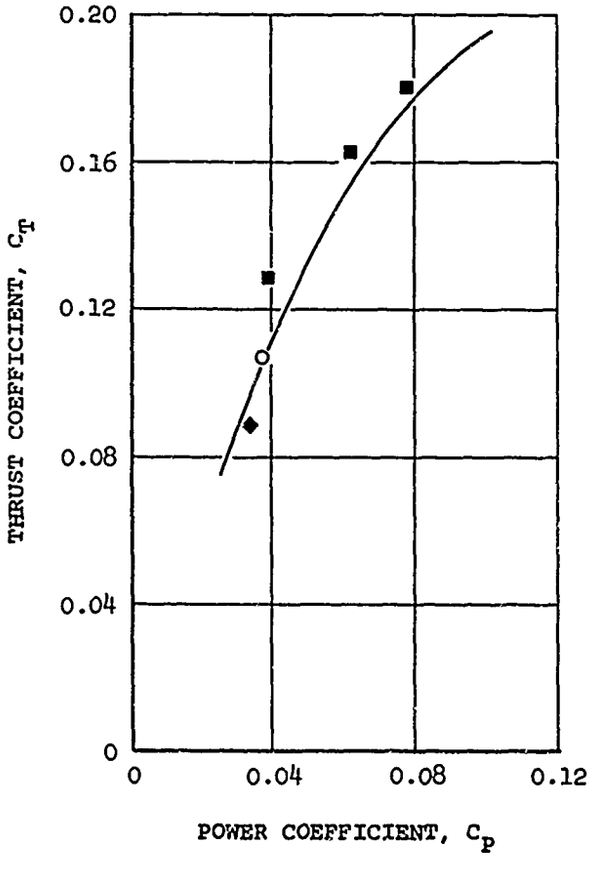

Figure 12. Thrust Coefficient Comparison.

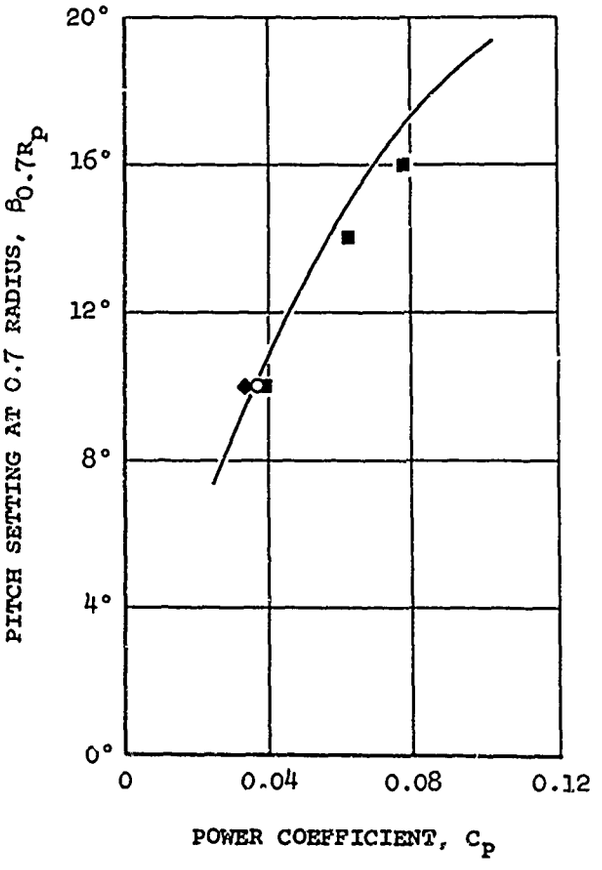

Figure 13. Pitch Setting Comparison.

3(109652) PROPELLER, ΩR_p = 785 fps

—— TEST CURVE, CURTISS STATIC TEST RIG
■ THEORETICAL POINT, INITIAL WAKE HYPOTHESIS
○ THEORETICAL POINT, REFINED WAKE HYPOTHESIS (K_u , K_v & K_w = ¼)
◆ THEORETICAL POINT, REFINED WAKE HYPOTHESIS (K_u , K_v & K_w = ½)

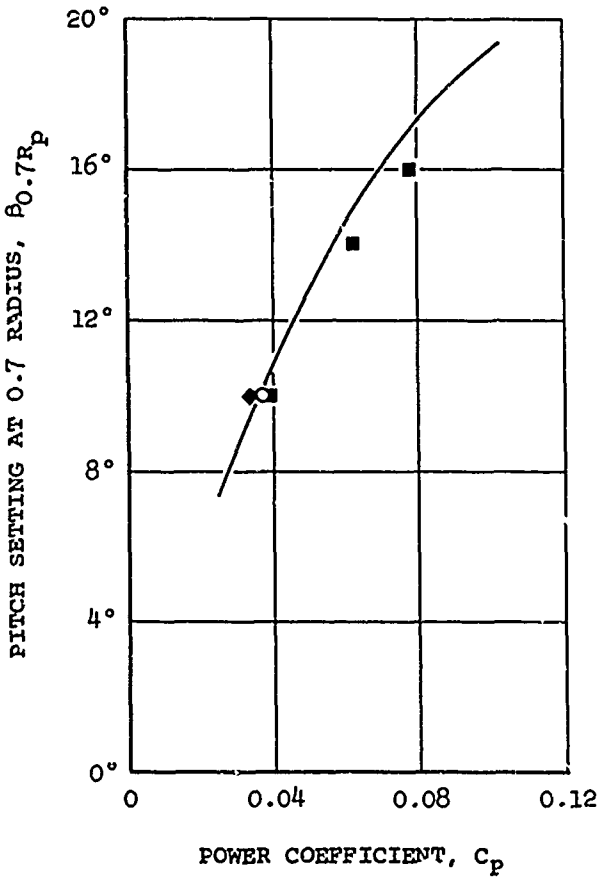

Figure 13. Pitch Setting Comparison.

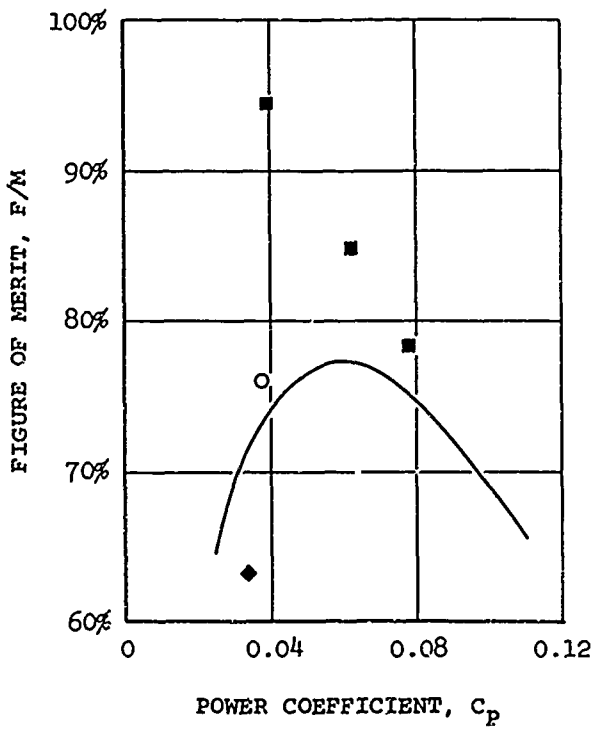

Figure 14. Figure of Merit Comparison.

B

TEST CURVE
THEORETICA

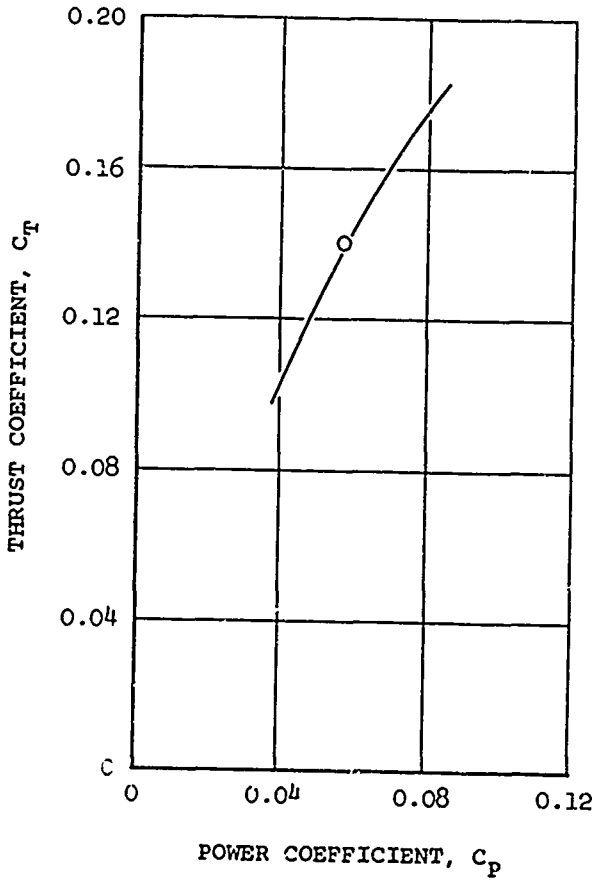

Figure 15. Thrust Coefficient Comparison.

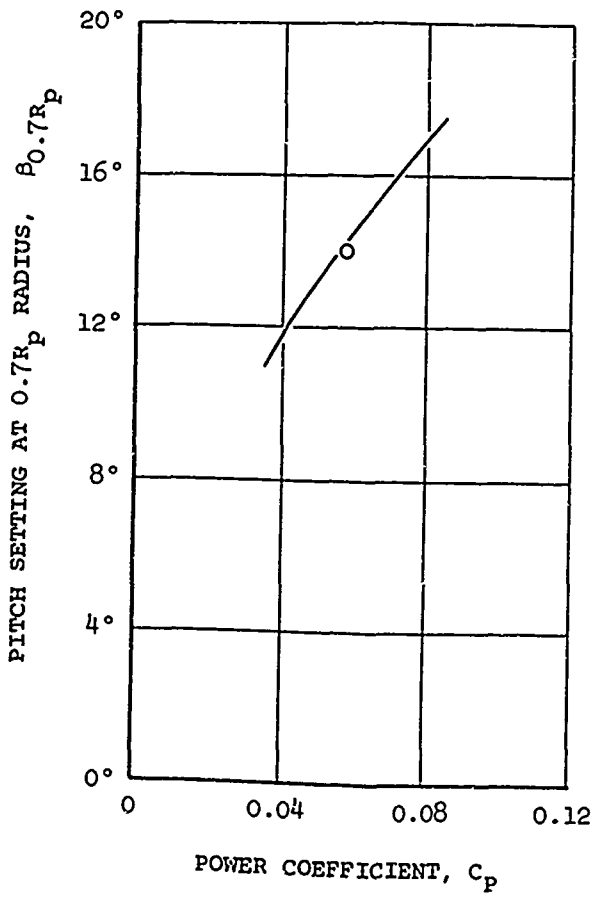

Figure 16. Pitch Setting Comparison.

3(13168A10P3) PROPELLER, ΩR_p = 750 fps

—— TEST CURVE, CURTISS STATIC TEST RIG

o THEORETICAL POINT, REFINED WAKE HYPOTHESIS (K_u & K_v = ¼)

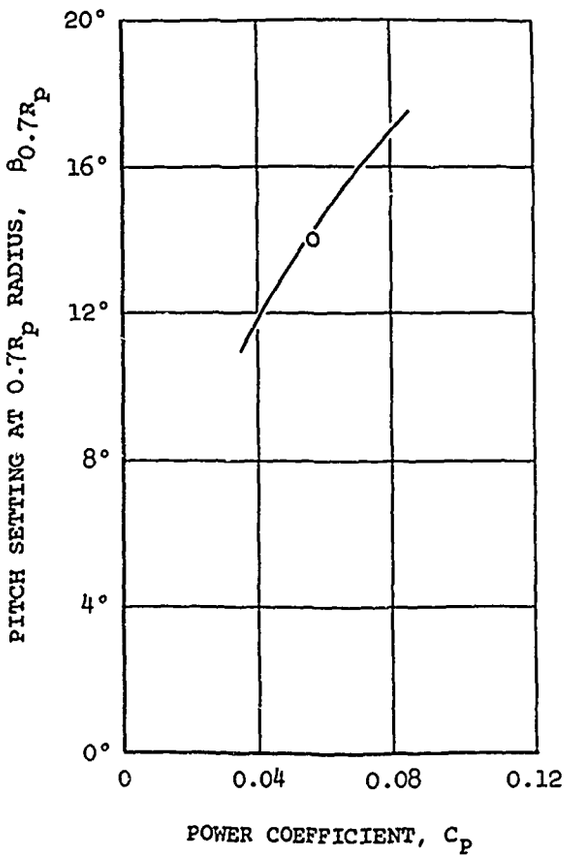

Figure 16. Pitch Setting Comparison.

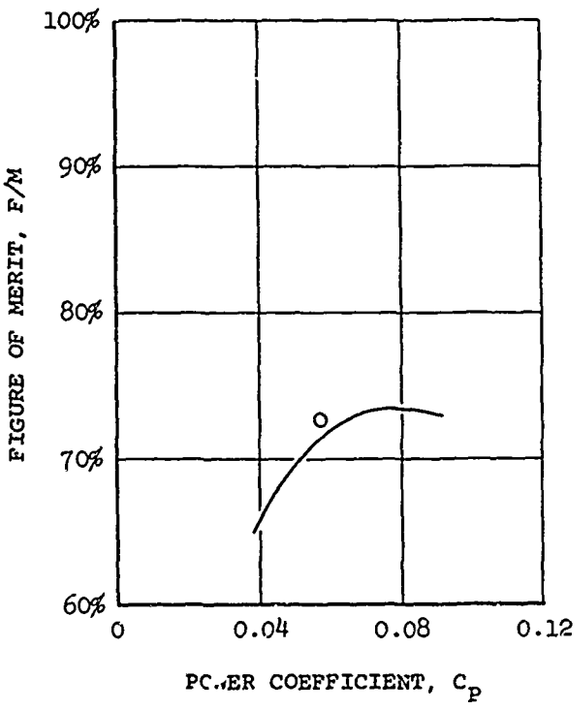

Figure 17. Figure of Merit Comparison.

B

TABLE 7

SUMMARY OF PERFORMANCE COMPARISONS

Propeller		Theory			Curtiss Test		
	C_P	C_T	$\beta_{0.7R_p}$	F/M	C_T	$\beta_{0.7R_p}$	F/M
3(109654)*	0.0477	0.141	11.3°	88.5%	0.131	10.7°	79.2%
3(109652)**	0.0370	0.107	10.0°	75.5%	0.105	10.2°	73.6%
3(13168A10P3)***	0.0576	0.140	14.0°	72.6%	0.138	14.3°	71.3%

* - Third Approximation, Initial Wake Hypothesis (K_u & K_v = ½)

** - First Approximation, Refined Wake Hypothesis (K_u , K_v & K_w = ¼)

*** - Third Approximation, Refined Wake Hypothesis (K_u & K_v = ¼)

The theoretical values are for the 3(109654) propeller, the third approximation using the initial wake hypothesis and iteration factors equal to one-half; for the 3(109652) propeller, the first approximation using the refined wake hypothesis and iteration factors equal to one-quarter; and for the 3(13168A10P3) propeller, the third approximation using the refined wake hypothesis and iteration factors equal to one-quarter.

As pointed out earlier, the comparisons for the 3(109654) propeller are unsatisfactory but those for the 3(109652) propeller are quite encouraging, although tentative. While the comparisons for the 3(13168A10P3) propeller are excellent, further approximations are still required.

CONCLUSIONS

Based on the results obtained in this study, we draw the following conclusions:

A model based on continuous deformation of the wake is necessary to calculate the inflow, and so the performance, of a V/STOL propeller at the static condition. The envelopes of the trajectories of the elements of the trailing vortex sheets and the "pitch" of these elements must be predicted accurately. An iteration procedure is used to solve the problem.

An initial wake hypothesis, or approximation to the force-free condition of the wake, gives a reasonable prediction of the trajectory envelopes, but an inadequate prediction of the "pitch". However, a refined wake hypothesis appears to give an adequate prediction of both the envelopes and the "pitch".

While the performance predictions for the 3(13168A10P3) propeller based on the refined wake hypothesis are excellent, further approximation(s) in the iteration procedure, as well as predictions at other pitch settings and for other propellers, are required. Comparison should also be made between the wake velocities used in the refined wake hypothesis and those found both by actual calculations and test measurements.

The main computer program which has been developed is very general. It can be utilized over a range of forward speeds and for a variety of applications other than the present problem. One such application which has been made is the calculation of input information for propeller-induced vibration of ship hulls.

RECOMMENDATIONS

Based on the results obtained in this study, we make the following recommendations:

Develop additional subroutines to incorporate the existing propeller airfoil data into the main computer program and introduce simplifications to shorten the time of preparation and running.

Make calculations of the induced velocity in the wake to examine in detail the refined wake hypothesis, or approximation to the force-free condition. Make corresponding full scale flow measurements to confirm the theoretical development. When this hypothesis is established or corrected, calculate solutions for three propellers at three pitch settings and compare with test data.

Calculate the inflow for four representative blade load distributions to provide an improved means for preliminary blade design estimates.

Determine the optimum circulation distribution for the static case analogous to the classical forward flight optimum.

BIBLIOGRAPHY

1. Abramowitz, M., and Stegun, I. A., Editors, Handbook of Mathematical Functions With Formulas, Graphs and Mathematical Tables, National Bureau of Standards, Applied Mathematics Series 55, Washington, D. C., 1964.

2. Anon., Operating Manual for Linear Constant-Temperature Hot-Film Anemometer Model 40W, Lintronic Laboratories, Ithaca, N. Y., 1963.

3. Borst, H. V., and Glover, L. S., Application of Theodorsen's Theory to Strip Analysis Procedure for Single Rotation Propellers, Report No. C-2070, Curtiss-Wright Corp., Propeller Div., Caldwell, N. J., September 2, 1949.

4. Byrd, P. F., and Friedman, M. D., Handbook of Elliptic Integrals for Engineers and Physicists, Springer-Verlag, Berlin, Germany, 1954.

5. Durand, W. F., Editor, Aerodynamic Theory, Vol. II, Dover Publications, Inc., New York, New York, 1963.

6. ibid., Vol. IV.

7. Enos, L. H., and Borst, H. V., Propeller Performance Analysis Aerodynamic Characteristics, NACA 16 Series Airfoils, Report No. C-2000, Curtiss-Wright Corp., Propeller Div., Caldwell, N. J., December 2, 1948.

8. Erickson, J. C., Jr., and Ordway, D. E., A New Approach to the Static Thrust Problem, Phase II, Calculation of Thrust and Torque, Model X-100 Propeller, $\beta_{0.7R_p} = 10.0°$, THERM, Incorporated, TAR-TR 632, May 1963.

9. Erickson, J. C., Jr., and Ordway, D. E., A New Approach to the Static Thrust Problem, Phase III, Further Inflow Calculations with Extensions to Partially Negative Γ Distributions, THERM, Incorporated, TAR-TR 635, August 1963.

10. Erickson, J. C., Jr., and Ordway, D. E., A New Approach to the Static Thrust Problem, Phase IV, Further Development of Performance Calculation Method, THERM, Incorporated, TAR-TR 638, December 1963.

11. Foss, R. L., Strip Analysis Method for Evaluating Static Thrust, Report No. C-2402, Curtiss-Wright Corp., Propeller Div., Caldwell, N. J., November 19, 1952.

12. Gail, A., Letter to the Editor, Journal of the Aeronautical Sciences, Volume 10, Number 8, October 1943, p. 320.

13. Glauert, H., The Elements of Aerofoil and Airscrew Theory, Second Edition, Cambridge University Press, Cambridge, England, 1948.

14. Hough, G. R., and Ordway, D. E., The Generalized Actuator Disk, Therm Advanced Research, Inc., TAR-TR 6401, January 1964; also "The Generalized Actuator Disk", Developments in Theoretical and Applied Mechanics, Volume II, Proceedings of the Second Southeastern Conference on Theoretical and Applied Mechanics, Pergamon Press, Oxford, England, 1965, pp. 317-336.

15. Iwasaki, M., Calculation of Static Thrust of Propellers(I), Private Communication, October 18, 1964.

16. Iwasaki, M., Calculation of Static Thrust of a Propeller(II), Private Communication, December 26, 1964.

17. Lin, C. C., Letter to the Editor, Journal of the Aeronautical Sciences, Volume 11, Number 3, July 1944, pp. 195-196.

18. Lock, C. N. H., The Application of Goldstein's Theory to the Practical Design of Airscrews, British ARC, R&M No. 1377, November 1930.

19. von Mises, R., Theory of Flight, Dover Publications, Inc., New York, New York, 1959.

20. Ordway, D. E., Sluyter, M. M., and Sonnerup, B. U. O., Three-Dimensional Theory of Ducted Propellers, THERM, Incorporated, TAR-TR 602, August 1960.

21. Ordway, D. E., and Greenberg, M. D., General Harmonic Solutions for the Ducted Propeller, THERM, Incorporated, TAR-TR 613, August 1961.

22. Ordway, D. E., and Erickson, J. C., Jr., A New Approach to the Static Thrust Problem, Phase I, Formulation and Preliminary Assessment of Mathematical Model, THERM, Incorporated, TAR-TR 631, March 1963.

23. Scarborough, J. B., Numerical Mathematical Analysis, The Johns Hopkins Press, Baltimore, Maryland, 1930.

24. Sears, W. R., Theoretical Aerodynamics, Part 1: Introduction to Theoretical Hydrodynamics, 1957 Edition, Ithaca, New York, 1957.

25. Theilheimer, F., Letter to the Editor, Journal of the Aeronautical Sciences, Volume 10, Number 8, October 1943, pp. 320-321.

26. Theodorsen, T., Theory of Propellers, McGraw-Hill, New York, New York, 1948.

27. Traub, J. F., Iterative Methods for the Solution of Equations, Prentice-Hall, Inc., Englewood Cliffs, New Jersey, 1964.

28. Wu, T. Y., "Flow Through a Heavily Loaded Actuator Disc", Schiffstechnik, Band 9, Heft 47, 1962, pp. 134-138.

APPENDIX I

OPERATING INSTRUCTIONS FOR COMPUTER PROGRAMS

General

Operating instructions for both the main computer program (CODEFVEL) as used for the Continuous Deformation Model and the short trajectory computer program (VORTTRAJ) are presented. These consist of descriptions of the input data required, their punch format and the print-out. It is assumed that the basic input data of the run are known: namely, the distributions of the blade circulation, the inflow velocity components and the velocity components along the trailing vortex sheets. All angles must be in radians and the remainder of the data must be nondimensionalized with respect to the characteristic time $1/\Omega$ and the characteristic length R_p .

Main Program (CODEFVEL)

Specify the number of propeller blades (NB), the propeller hub radius (RBH), the total number of field points (NTIP) desired, and the axial (XB), radial (RB) and azimuthal (TB) coordinates of the field points. The field points cannot exceed 20 and must be numbered consecutively for identification, starting from that point on a propeller blade nearest the hub and proceeding along the blade, followed by points off the blades.

Use the following values: for (IDIS), 3; for (T), (TIR), (TOR) and (DTREG), all 0.0; for (INDEX), 1; and for (NREG) and (IDVP), both 0 .

Specify for the blade circulation distribution the number of Glauert coefficients (NC), the maximum value of the circulation (GD) and the values of the circulation (GB) at the total number (NG) of radial stations (RG). NC cannot exceed 20 and NG cannot exceed 30 .

Specify the absolute value of accuracy (TOL) required in the Gaussian integration scheme and the maximum number of subdivisions (NLIMIT) permitted before termination.

Normalize the velocity components at points along the trailing

vortex sheets with respect to the corresponding values in the propeller plane at the same radius. Specify the normalized axial (UB), radial (VB) and tangential (WB) velocity components at 15 radial stations (R) for each of 20 axial stations (X). Specify the magnitudes of the axial (UD), radial (VD) and tangential (WD) inflow components at the propeller plane for the same 15 radial stations.

Specify the step sizes (DTOIC and DTICDH) of the first and second time increments in the marching scheme, the number of steps at each (NIOIC and NIICDH) and the ratio (NR) of DTICDH to DTOIC. NR must be an integer. Determine the time elapsed during the march (TDH) by adding the product of NIOIC and DTOIC to the product of NIICDH and DTICDH. Set the quantities TDHI and TDHO, the elapsed time (TA) after which the asymptotic formulas of the influence functions are picked up, and the quantities TAI and TAO all equal to the value of TDH. Specify the absolute value of accuracy (TOLS) required in computing the Heuman lambda function (use 0.0001).

Specify the total number of trailing vortex elements (NVP) required for computing the integrands of Eqs. (2) to (4) and their initial radial coordinates (RBP) as they leave the blades. Set their initial axial (XBP) and azimuthal (TBP) coordinates equal to 0.0 . Number the vortex elements consecutively from 1, which must coincide with the hub, to NVP, which must coincide with the tip. NVP cannot exceed 108 . Specify, for each vortex element, the total number of field points (NIP) at which the influence functions for this element are desired and the index numbers of these points (INIP). Specify correspondingly, for each field point, the total number of vortex elements (NIVP) contributing influence functions and the index numbers of these elements (IVP). Check NIP, INIP, NIVP and IVP for consistency.

Specify the total number of vortex elements (NPVP) at which intermediate trajectory and influence function print-out is desired and the index numbers of these elements (IPVP). If none is desired, set NPVP equal to 1 and IPVP(1) equal to 0

The punch format for program CODEFVEL is given in Table 8 and includes the input quantities, the field specification and the number of cards required.

The print-out of program CODEFVEL is comprehensive and consists, in general, of the following: the axial, radial and tangential velocity components in the stored input field; identification of the field points; the Glauert coefficients and values for the representation of the circulation and its

TABLE 8

INPUT PUNCH FORMAT - PROGRAM CODEFVEL

Input Quantity	Field Spec.	No. Of Cards
X(1) - X(10) X(11) - X(20)	F8	2
R(1) - R(10) R(11) - R(15)	F8	2
UB(X1,R1) - UB(X10,R1) UB(X11,R1) - UB(X20,R1) . . . UB(X1,R15) - UB(X10,R15) UB(X11,R15) - UB(X20,R15)	F8	30
VB(X1,R1) - VB(X10,R1) VB(X11,R1) - VB(X20,R1) . . . VB(X1,R15) - VB(X10,R15) VB(X11,R15) - VB(X20,R15)	F8	30
WB(X1,R1) - WB(X10,R1) WB(X11,R1) - WB(X20,R1) . . . WB(X1,R15) - WB(X10,R15) WB(X11,R15) - WB(X20,R15)	F8	30
NC, NTIP, NVP, NB, NLIMIT, NG, IDIS	I5	1
UD(1) - UD(10) UD(11) - UD(15) VD(1) - VD(10) VD(11) - VD(15) WD(1) - WD(10) WD(11) - WD(15)	F8	6

TABLE 8 - contd.

TDHI, TDHO, TAI, TAO, GD, RBH, TOL, TOLS, TIR, TOR	F8	1
XB(1) - XB(10) XB(11) - XB(NTIP)	F8	*
RB(1) - RB(10) RB(11) - RB(NTIP)	F8	*
TB(1) - TB(10) TB(11) - TB(NTIP)	F8	*
GB(1) - GB(10) GB(11) - GB(NG)	F8	*
RG(1) - RG(10) RG(11) - RG(NG)	F8	*
NPVP, IPVP(1) - IPVP(15) IPVP(16) - IPVP(NPVP)	I5	*
DTOIC, DTICDH, DTREG, T, TDH, TA	F8	1
INDEX, NIOIC, NIICDH, NR, NREG, IDVP	I5	1
XBP, RBP, TBP	F8	**
NIP, INIP(1) - INIP(15) INIP(16) - INIP(NIP)	I5	**
NIVP, IVP(1) - IVP(15) IVP(16) - IVP(NIVP)	I5	***

* - As Many as Required
** - One Set of as Many as Required for Each Vortex Element
*** - One Set of as Many as Required for Each Field Point

derivative with respect to the Glauert variable; the strengths of the Cauchy and logarithmic singularities as defined in Eqs. (24) to (26); the successive values, as the Gaussian integration scheme subdivides, of the contribution of the bound blade vortices to the induced velocity components at each field point off the blades; the contribution from the bound blade vortices to the induced velocity components; the regular part of the integrand in Eqs. (2) to (4) from the trailing vortex sheets; the successive values, as the Gaussian integration scheme subdivides, of the contribution of the regular part to the induced velocity components at each field point; the sum of the contributions from the regular part and from the bound blade vortices to the induced velocity components; the contribution from the Cauchy singularity of the influence functions of the trailing vortex sheets to the induced velocity components; the contribution from the logarithmic singularity to the induced velocity components; the resulting total singular contribution to the induced velocity components; and the final values for the induced velocity components. The intermediate print-out for each specified vortex element consists of the following: the coordinates and velocity components at every other step of the march along the trajectory; the same quantities at the termination of the march; the contribution to the influence functions at the specified field points by integration to the end of the march; the total influence functions at the specified field points; and the regular parts of these influence functions.

Trajectory Program (VORTTRAJ)

Specify (UB), (VB), (WB), (X), (R), (UD), (VD), (WD), (DTOIC), (DTICDH), (NIOIC), (NIICDH), (NR), (NVP), (XBP), (RBP) and (TBP) in the same fashion as for program CODEFVEL . Specify further the total number of sets (NVF) of inflow fields UD, VD and WD that are desired. NVF cannot exceed 20 and here NVP cannot exceed 100 .

The punch format for program VORTTRAJ is given in Table 9 and includes the input quantities, the field specification and the number of cards required.

The print-out of program VORTTRAJ consists of the following: the axial, radial and tangential velocity components in the stored input field; and at every other step of the march along each trajectory, the coordinates, including the projection $(r_v/R_p) \cos \theta_v$, and the velocity components.

TABLE 9

INPUT PUNCH FORMAT - PROGRAM VORTRAJ

Input Quantity	Field Spec.	No. Of Cards
NVP, NVF, NIOIC, NIICDH, NR	I5	1
X(1) - X(10) X(11) - X(20)	F8	2
R(1) - R(10) R(11) - R(15)	F8	2
UB(X1,R1) - UB(X10,R1) UB(X11,R1) - UB(X20,R1) . . . UB(X1,R15) - UB(X10,R15) UB(X11,R15) - UB(X20,R15)	F8	30
VB(X1,R1) - VB(X10,R1) VB(X11,R15) - VB(X20,R1) . . . VB(X1,R15) - VB(X10,R15) VB(X11,R15) - VB(X20,R15)	F8	30
WB(X1,R1) - WB(X10,R1) WB(X11,R1) - WB(X20,R1) . . . WB(X1,R15) - WB(X10,R15) WB(X11,R15) - WB(X20,R15)	F8	30

TABLE 9 - contd.

UD(R1,1) - UD(R10,1) UD(R11,1) - UD(R15,1) VD(R1,1) - VD(R10,1) VD(R11,1) - VD(R15,1) WD(R1,1) - WD(R10,1) WD(R11,1) - WD(R15,1) . . . UD(R1,NVF) - UD(R10,NVF) UD(R11,NVF) - UD(R15,NVF) VD(R1,NVF) - VD(R10,NVF) VD(R11,NVF) - VD(R15,NVF) WD(R1,NVF) - WD(R10,NVF) WD(R11,NVF) - WD(R15,NVF)	F8	*
XBP(1), RBP(1), TBP(1) . . . XBP(NVP), RBP(NVP), TBP(NVP)	F8	NVP
DTOIC, DTICDH	F8	1

* - Six Times NVF

APPENDIX II

BLADE CHARACTERISTICS

All three propellers considered in the text for both theoretical calculations and comparison with test data, namely the 3(109654), 3(109652) and 3(13168A10P3) propellers, have three blades, as indicated by the digit 3 in front of the designations. The digits and letters within the parentheses refer to the blade design. The geometries and characteristics of these three blade designs are given in Figs. 18, 19 and 20, with h/b as the local blade thickness-to-chord ratio and

$$AF \equiv \frac{100,000}{16} \int_{0.2}^{1.0} \frac{b}{2R_p} \left(\frac{r_p}{R_p}\right)^3 d\left(\frac{r_p}{R_p}\right) \tag{27}$$

$$IC_{L_i} \equiv 4 \int_{0.2}^{1.0} C_{L_i} \left(\frac{r_p}{R_p}\right)^3 d\left(\frac{r_p}{R_p}\right) \tag{28}$$

where

AF is the activity factor of the blade,

IC_{L_i} is the integrated design lift coefficient of the blade and

C_{L_i} is the blade sectional design lift coefficient (Ref. 7, pp. 2 to 5, for example).

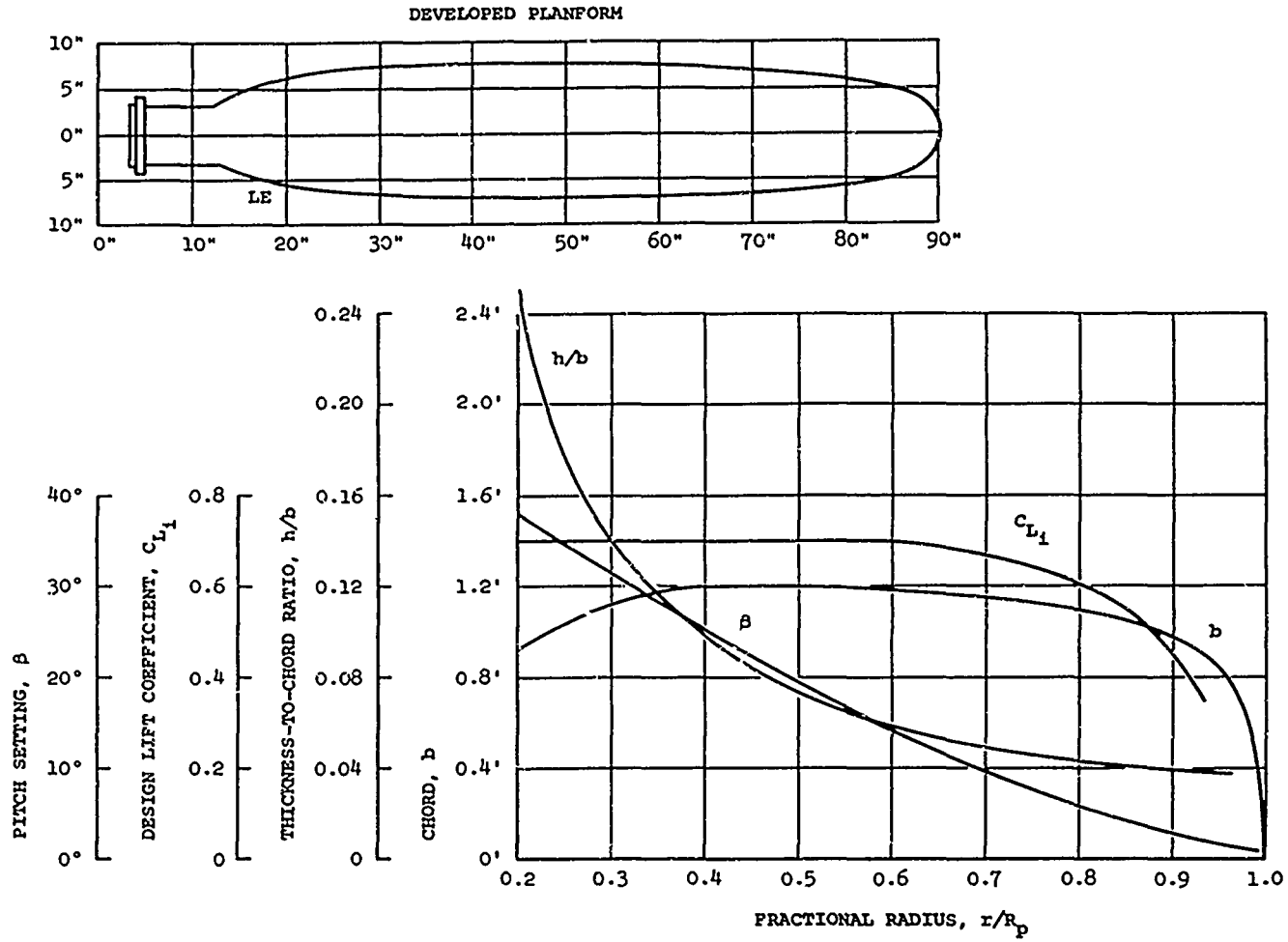

Figure 18. Blade Characteristics, 109654 Design. NACA 16-Series Sections, $2R_p$ = 15'1" , AF = 105 , IC_{L_i} = 0.505 .

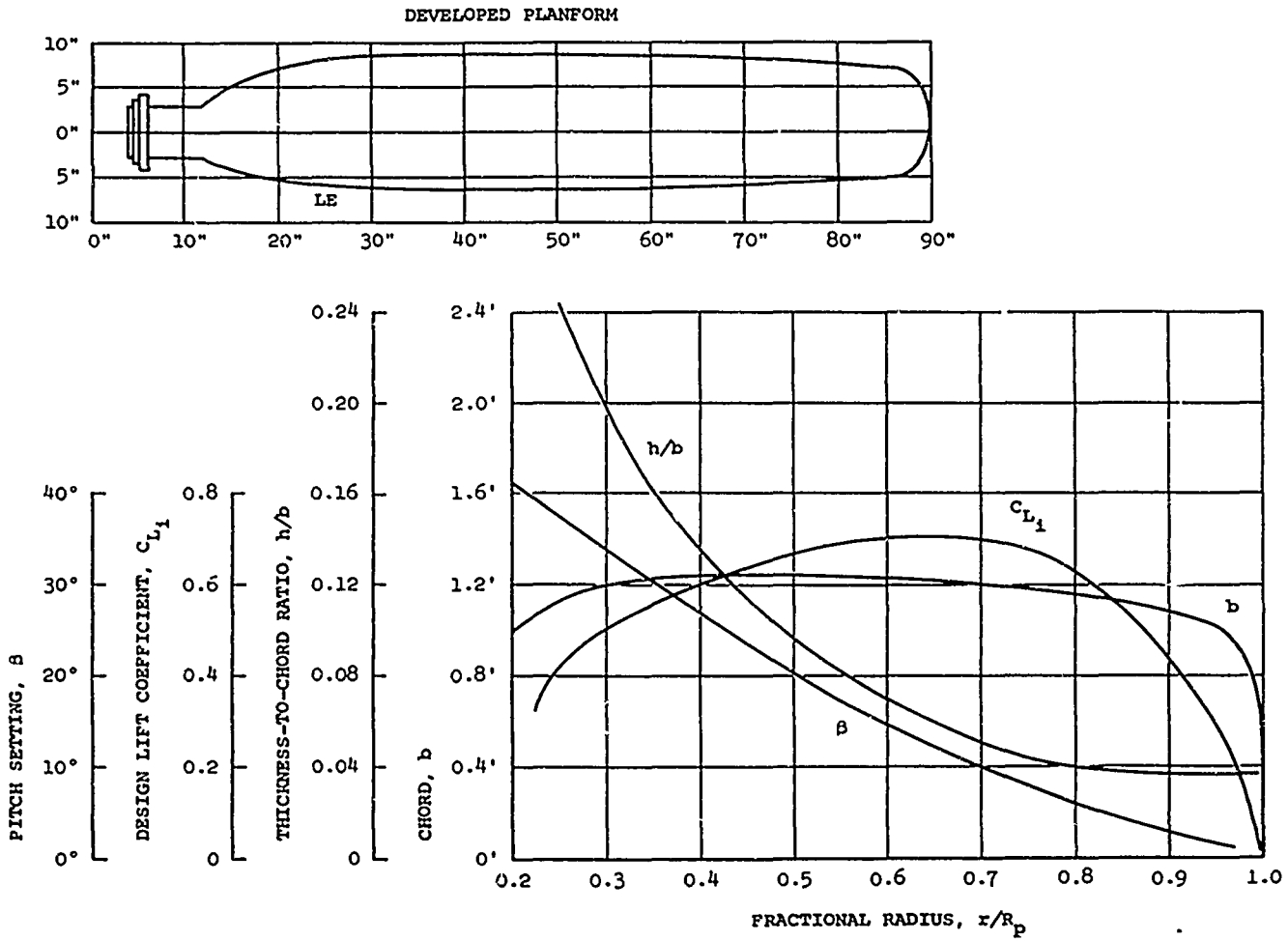

Figure 19. Blade Characteristics, 109652 Design. NACA 65-Series Sections, $2R_p$ = 15'0" , AF = 115 , IC_{L_i} = 0.500 .

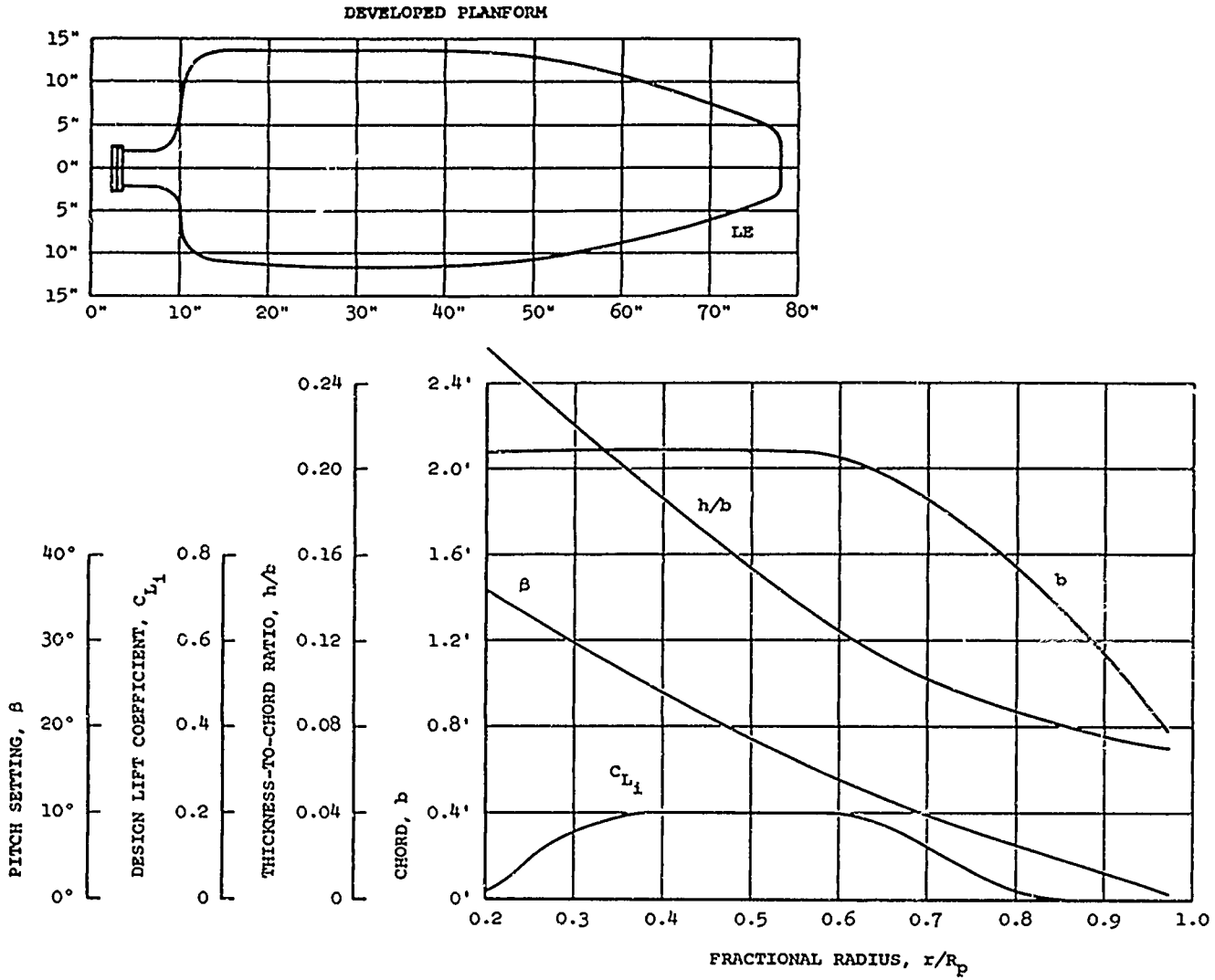

Figure 20. Blade Characteristics, 13168A10P3 Design. NACA 64-Series Sections, $2R_p$ = 13'0" , AF = 168 , IC_{L_i} = 0.057 .

UNCLASSIFIED
Security Classification

DOCUMENT CONTROL DATA - R&D
(Security classification of title, body of abstract and indexing annotation must be entered when the overall report is classified)

1. ORIGINATING ACTIVITY (Corporate author)	2a. REPORT SECURITY CLASSIFICATION
Curtiss-Wright Corp., VTOL Systems Division Therm Advanced Research, Inc.	Unclassified
	2b GROUP —

3. REPORT TITLE

A THEORY FOR VTOL PROPELLER OPERATION IN A STATIC CONDITION

4. DESCRIPTIVE NOTES (Type of report and inclusive dates)

Final Report, June 1964 - May 1965

5. AUTHOR(S) (Last name, first name, initial)

Erickson, John C. Jr., Ladden, Richard M.,
Borst, Henry V., Ordway, Donald E.

6. REPORT DATE	7a. TOTAL NO OF PAGES	7b. NO. OF REFS
October 1965	76	28

8a. CONTRACT OR GRANT NO.	9a. ORIGINATOR'S REPORT NUMBER(S)
DA44-177-AMC-165(T) b. PROJECT NO. 1M121401D14415 c. d.	USAAVLABS Technical Report 65-69 9b. OTHER REPORT NO(S) (Any other numbers that may be assigned this report) —

10. AVAILABILITY/LIMITATION NOTICES

Qualified requesters may obtain copies of this report from DDC. This report has been furnished to the Department of Commerce for sale to the public.

11. SUPPLEMENTARY NOTES	12. SPONSORING MILITARY ACTIVITY
—	U. S. Army Aviation Materiel Laboratories Fort Eustis, Virginia

13. ABSTRACT

A general theory for calculation of propeller performance at the static condition has been formulated based on a continuous vortex representation along the lines of the classical lifting-line model. As opposed to forward flight, the deformation of the wake is appreciable just behind the propeller, and its determination constitutes the heart of the static problem. A computer program has been developed to calculate both the inflow at the propeller and the induced velocity at any field point for an arbitrary description of the trailing vortex sheets. To approximate the force-free condition imposed on the wake, an initial wake hypothesis derived from the theory of the Generalized Actuator Disk was first used. It led to unsatisfactory comparisons with test measurements and a refined wake hypothesis was derived. The refined wake hypothesis provides a more reasonable representation of the "pitch" of the elements of the deformed trailing vortex sheets as well as the envelope of their trajectories. Comparisons at one power coefficient show excellent agreement with test data; the discrepancy in thrust, pitch setting and figure of merit is about 1%, 2% and 1%, respectively.

DD FORM 1 JAN 64 1473

UNCLASSIFIED
Security Classification

UNCLASSIFIED
Security Classification

14. KEY WORDS	LINK A		LINK B		LINK C	
	ROLE	WT	ROLE	WT	ROLE	WT
Propeller Theory						
Static Performance						
Propeller Tests						
VTOL						

INSTRUCTIONS

1. ORIGINATING ACTIVITY: Enter the name and address of the contractor, subcontractor, grantee, Department of Defense activity or other organization *(corporate author)* issuing the report.

2a. REPORT SECURITY CLASSIFICATION: Enter the overall security classification of the report. Indicate whether "Restricted Data" is included. Marking is to be in accordance with appropriate security regulations.

2b. GROUP: Automatic downgrading is specified in DoD Directive 5200.10 and Armed Forces Industrial Manual. Enter the group number. Also, when applicable, show that optional markings have been used for Group 3 and Group 4 as authorized.

3. REPORT TITLE: Enter the complete report title in all capital letters. Titles in all cases should be unclassified. If a meaningful title cannot be selected without classification, show title classification in all capitals in parenthesis immediately following the title.

4. DESCRIPTIVE NOTES: If appropriate, enter the type of report, e.g., interim, progress, summary, annual, or final. Give the inclusive dates when a specific reporting period is covered.

5. AUTHOR(S): Enter the name(s) of author(s) as shown on or in the report. Enter last name, first name, middle initial. If military, show rank and branch of service. The name of the principal author is an absolute minimum requirement.

6. REPORT DATE: Enter the date of the report as day, month, year; or month, year. If more than one date appears on the report, use date of publication.

7a. TOTAL NUMBER OF PAGES: The total page count should follow normal pagination procedures, i.e., enter the number of pages containing information.

7b. NUMBER OF REFERENCES: Enter the total number of references cited in the report.

8a. CONTRACT OR GRANT NUMBER: If appropriate, enter the applicable number of the contract or grant under which the report was written.

8b, 8c, & 8d. PROJECT NUMBER: Enter the appropriate military department identification, such as project number, subproject number, system numbers, task number, etc.

9a. ORIGINATOR'S REPORT NUMBER(S): Enter the official report number by which the document will be identified and controlled by the originating activity. This number must be unique to this report.

9b. OTHER REPORT NUMBER(S): If the report has been assigned any other report numbers *(either by the originator or by the sponsor)*, also enter this number(s).

10. AVAILABILITY/LIMITATION NOTICES: Enter any limitations on further dissemination of the report, other than those imposed by security classification, using standard statements such as:

(1) "Qualified requesters may obtain copies of this report from DDC."

(2) "Foreign announcement and dissemination of this report by DDC is not authorized."

(3) "U. S. Government agencies may obtain copies of this report directly from DDC. Other qualified DDC users shall request through _____."

(4) "U. S. military agencies may obtain copies of this report directly from DDC. Other qualified users shall request through _____."

(5) "All distribution of this report is controlled. Qualified DDC users shall request through _____."

If the report has been furnished to the Office of Technical Services, Department of Commerce, for sale to the public, indicate this fact and enter the price, if known.

11. SUPPLEMENTARY NOTES: Use for additional explanatory notes.

12. SPONSORING MILITARY ACTIVITY: Enter the name of the departmental project office or laboratory sponsoring *(paying for)* the research and development. Include address.

13. ABSTRACT: Enter an abstract giving a brief and factual summary of the document indicative of the report, even though it may also appear elsewhere in the body of the technical report. If additional space is required, a continuation sheet shall be attached.

It is highly desirable that the abstract of classified reports be unclassified. Each paragraph of the abstract shall end with an indication of the military security classification of the information in the paragraph, represented as *(TS), (S), (C), or (U)*.

There is no limitation on the length of the abstract. However, the suggested length is from 150 to 225 words.

14. KEY WORDS: Key words are technically meaningful terms or short phrases that characterize a report and may be used as index entries for cataloging the report. Key words must be selected so that no security classification is required. Identifiers, such as equipment model designation, trade name, military project code name, geographic location, may be used as key words but will be followed by an indication of technical context. The assignment of links, rules, and weights is optional.

UNCLASSIFIED
Security Classification

6515-65